37564-6001-UT-00

MICROWAVE BACKSCATTERING FROM SHORT GRAVITY WAVES: A DETERMINISTIC, COHERENT AND DUAL-POLARIZED LABORATORY STUDY

by

DANIEL S. W. KWOH
BRUCE M. LAKE

JULY 1983

Prepared for

Office of Naval Research
Coastal Sciences Program
Contract No. N00014-C-81-0217
Project NR 387-133
NR 083-556X

Approved for public release, distribution unlimited

TRW
SPACE AND TECHNOLOGY GROUP
ONE SPACE PARK
REDONDO BEACH, CALIFORNIA 90278

37564-6001-UT-00

MICROWAVE BACKSCATTERING FROM SHORT GRAVITY WAVES: A DETERMINISTIC, COHERENT AND DUAL-POLARIZED LABORATORY STUDY

by

DANIEL S. W. KWOH
BRUCE M. LAKE

JULY 1983

Prepared for

Office of Naval Research
Coastal Sciences Program
Contract No. N00014-C-81-0217
Project NR 387-133
NR 083-556X

Approved for public release, distribution unlimited

TRW
SPACE AND TECHNOLOGY GROUP
ONE SPACE PARK
REDONDO BEACH, CALIFORNIA 90278

UNCLASSIFIED

SECURITY CLASSIFICATION OF THIS PAGE (When Data Entered)

REPORT DOCUMENTATION PAGE

READ INSTRUCTIONS BEFORE COMPLETING FORM

1. REPORT NUMBER: TRW Report No. 37564-6001-UT-00

2. GOVT ACCESSION NO.:

3. RECIPIENT'S CATALOG NUMBER:

4. TITLE (and Subtitle): Microwave Backscattering from Short Gravity Waves: A Deterministic; Coherent and Dual-Polarized Laboratory Study

5. TYPE OF REPORT & PERIOD COVERED: Status, 5-1-81 to 5-1-82

6. PERFORMING ORG. REPORT NUMBER:

7. AUTHOR(s):
Daniel S. W. Kwoh
Bruce M. Lake

8. CONTRACT OR GRANT NUMBER(s): N00014-81-C-0217

9. PERFORMING ORGANIZATION NAME AND ADDRESS:
Fluid Mechanics Department
TRW Space and Technology Group, One Space Park,
Redondo Beach, CA 90278

10. PROGRAM ELEMENT, PROJECT, TASK AREA & WORK UNIT NUMBERS:
NR 387-133
NR 083-556X

11. CONTROLLING OFFICE NAME AND ADDRESS:
Office of Naval Research
Coastal Sciences Program
Arlington, VA 22217

12. REPORT DATE: May 1982

13. NUMBER OF PAGES: 80

14. MONITORING AGENCY NAME & ADDRESS (if different from Controlling Office):

15. SECURITY CLASS. (of this report): Unclassified

15a. DECLASSIFICATION/DOWNGRADING SCHEDULE:

16. DISTRIBUTION STATEMENT (of this Report)

Approved for public release; distribution unlimited

17. DISTRIBUTION STATEMENT (of the abstract entered in Block 20, if different from Report)

18. SUPPLEMENTARY NOTES

19. KEY WORDS (Continue on reverse side if necessary and identify by block number)
Microwave Backscattering
Deep-Water Gravity Waves

20. ABSTRACT (Continue on reverse side if necessary and identify by block number)

The fundamental mechanisms of microwave backscattering from short gravity waves are investigated in the laboratory using a cw coherent dual-polarized focused radar and a laser scanning slope gauge which provides an almost instantaneous profile of the water surface while scattering is taking place. The surface is also monitored independently for specular reflection using an optical sensor. It is found that microwave backscattering occurs in discrete bursts which are highly correlated with "gentle" breaking of the waves. These backscattering
(Cont. on reverse side)

DD FORM 1 JAN 73 1473 EDITION OF 1 NOV 65 IS OBSOLETE
S/N 0102-LF-014-6601

UNCLASSIFIED
SECURITY CLASSIFICATION OF THIS PAGE (When Data Entered)

20. Abstract (Cont.)

bursts are either completely nonspecular or are partially specular in nature. The specular contribution is found to be more important than generally expected, even at moderate to high incidence angles, and its source seems to be the specular facets in the turbulent wake and the capillary waves generated during breaking. Completely nonspecular backscattering bursts are analyzed by using the Method of Moments to numerically compute the backscattering complex amplitudes from the measured profiles and then comparing the computed results with the measured results. Using numerical modeling, it can be shown that for a wave in the process of breaking, its small-radius crest is the predominant scattering source in a manner akin to wedge diffraction as described by the Geometric Theory of Diffraction (GTD). The parasitic capillary waves generated during wave breaking also scatter. Their contribution is in general smaller than that of the crest and can be understood in terms of small perturbation theory. The relationship between GTD and small perturbation theory in the description of wedge diffraction is established. Implications of our work for microwave backscatter from the ocean surface are examined.

TABLE OF CONTENTS

Acknowledgement

The authors would like to thank Peter Lee for leaving us a radar system that works, Dewey Rowland, Rudy Acosta, Brian McGee, and Ernie Hoover for assistance in the course of the work, Jim Sherman for designing the slope gauge electronics, Dick Wagner for first lending us his laser slope gauge and later helping us to modify it into the scanning version, and Hans Dolezalek for encouragement and critical comments.

Abstract

The fundamental mechanisms of microwave backscattering from short gravity waves are investigated in the laboratory using a cw coherent dual-polarized focused radar and a laser scanning slope gauge which provides an almost instantaneous profile of the water surface while scattering is taking place. The surface is also monitored independently for specular reflection using an optical sensor. It is found that microwave backscattering occurs in discrete bursts which are highly correlated with "gentle" breaking of the waves. These backscattering bursts are either completely nonspecular or are partially specular in nature. The specular contribution is found to be more important than generally expected, even at moderate to high incidence angles, and its source seems to be the specular facets in the turbulent wake and the capillary waves generated during breaking. Completely nonspecular backscattering bursts are analyzed by using the Method of Moments to numerically compute the backscattering complex amplitudes from the measured profiles and then comparing the computed results with the measured results. Using numerical modeling, it can be shown that for a wave in the process of breaking, its small-radius crest is the predominant scattering source in a manner aking to wedge diffraction as described by the Geometric Theory of Diffraction (GTD). The parasitic capillary waves generated during wave breaking also scatter. Their contribution is in general smaller than that of the crest and can be understood in terms of small perturbation theory. The relationship between GTD and small perturbation theory in the description of wedge diffraction is established. Implications of our work for microwave backscattering from the ocean surface are examined.

EXECUTIVE SUMMARY

During the past ten years, the "composite model" has become increasingly accepted as the correct theory for the description of microwave scattering from the ocean surface. The basic premise of the theory is that microwave radiation (at moderate to large incidence angles) backscatters from "slightly rough" patches which are created by wind on the ocean surface. These patches are geometrically tilted by the underlying gravity waves and they also interact dynamically with the wind, the wind drift layer and the orbital current of underlying gravity waves. The electromagnetic theory that describes the scattering mechanism was developed by Rice[1]. The microwave radiation is assumed to scatter selectively from a Fourier component of the "slightly rough" surface which satisfies the Bragg condition. The theory that describes the interaction between this Bragg component and other wave components and currents and wind has gone through various stages of development to reach its present rather elaborate form as described by Hasselmann[2] and Wright et al[3].

Our recent laboratory study shows that Bragg scattering by itself is not an adequate description for microwave backscattering from water waves. It may account for part of the scattering, but reflection from specular facets and wedge-like diffractive scattering from small radius crests of waves can predominate.

Our experiments were performed on wave paddle-generated short gravity waves without wind (later experiments will add wind to the system). We have investigated x-band backscattering at moderate incidence angles using a CW coherent dual-polarized focused radar and a laser scanning slope gauge which provides an almost instantaneous profile of the water surface during scattering.

We have used a deterministic rather than a statistical approach. The surface was also independently monitored for specular reflections. We also used the moments method to numerically compute backscattering complex amplitudes from the measured profiles. Comparisons between the measured backscattering amplitudes and those computed using both measured and modeled wave profiles shows that the small radius crests of such waves can be the more dominant source of scattering and that the description of such scattering is closer to wedge diffraction than to Bragg scattering. Bragg scattering does describe the scattering from the parasitic capillaries. We also find that specular reflection is more important than generally expected.

More specifically, we have found that for water wave trains with small amplitude, there is hardly any measurable microwave backscattering. As wave amplitude is increased, however, beyond a certain threshold, backscattering quickly appears. This threshold corresponds to the onset of self-modulation in the wave train. At a steepness of ka = 0.17, the self-modulation is such that at 8.4 m fetch, one out of every three or four waves attains a small enough radius of curvature at the crest that it undergoes breaking with capillary waves being radiated down the front face. A turbulent wake may or may not appear behind the crest. We refer to this kind of breaking as "gentle breaking" since it does not involve bubbles or spray. For wave trains under these conditions, we observe that the backscattering occurs as discrete bursts (rather than as a white-noise-like continuous return) and the bursts strongly correlate with the "gentle breaking" events. The discreteness of the bursts implies that the scattering sources are localized on the surface. These discrete scattering events have been carefully studied and can be separated into two categories: (a) nonspecular events, and (b) specular events, which may have a small hidden nonspecular component.

The specular events have been studied with the aid of flash photography. We have found that the frequency of specular events varies from roughly one third of all events at 40° incidence to roughly one sixth of all events at 67.7° incidence angle. The power of a typical specular event is usually two or more times higher than that of a typical nonspecular event. The polarization ratios of specular events at 40° and 55° incidence angles are very close to 0 db. At 67.7°, the ratio is slightly higher. The occurrence of specular events like these may be the primary reason for the ocean polarization ratios being closer to 0 db than expected. The Doppler shift of specular events indicates a surface velocity close to the phase velocity of the short gravity waves, i.e., $\sim$62.5 cm/sec (or approximately double the phase velocity of Bragg wavelets under these conditions). Our flash photographs show that specular reflection comes either from a very turbulent wake, in which case bright dots appear in the picture, or from steep capillaries, in which case lines or rings appear in the flash picture. Although our brief study here does not do justice to the importance of specular reflection, it does serve to point out that the potential significance of specular backscattering from the ocean at moderate incidence angles ought to be investigated.

The nonspecular events have been investigated using the deterministic approach. We have demonstrated the feasibility of the deterministic approach by comparing the measured results with numerically computed results in terms of absolute backscattered power, polarization ratio and Doppler shift. Having thus validated the approach, we have used it to show that the background wave form is the dominant scattering source, and that it scatters in a manner not describable by the small perturbation theory (SPT). A better description may be that of a wedge (describable by the geometric theory of diffraction, or GTD)

with a rounded tip (describable by SPT, which reduces scattering by about 6 db) and a concave front face (describable by SPT, which increases scattering by about 2 db). We have established that the wedge-like character of the crest is the reason that the background wave form is not describable by SPT. It is also probably the second reason why the ocean polarization ratio is smaller than expected. The Doppler shift associated with the background wave form corresponds to the phase speed of the short gravity waves, i.e., ~62.5 cm/sec in our cases. The parasitic capillaries also scatter, but their contribution is usually a few db smaller than that of the background wave form and it may be in or out of phase with the background wave form. The polarization ratios measured at all incidence angles are smaller than those obtained if scattering came solely from capillaries on inclined planes scattering in the SPT manner, which is consistent with our results for the scattering contribution of the background wave form. The Doppler shift associated with the capillaries corresponds to speeds within ± 10% of the gravity wave phase speeds, an indication of the parasitic nature of such capillary waves. The parasitic capillary scattering can be completely understood in terms of SPT although the dominant wavelength of the capillaries is far from being "resonant" with x-band at moderate incidence angles. We can say that it is the capillary induced surface roughness which is scattering in a small perturbation manner. One implication is that Ka-band or higher microwave frequencies may be better frequencies for sensing these parasitic capillaries. Another implication is that for frequencies lower than x-band, say L-band, the scattering will become more wedge-like in character. (Of course, in the limit of even lower frequency, SPT will become applicable again at some point.)

Our study of mechanically-generated wave trains is intended to be a first step in the study of progressively more complicated and more realistic

wave systems. It is our hope that the knowledge gained at each step will help us decipher the scattering signatures in the next. A detailed study of scattering from wind waves in the laboratory will be presented in a later report. At this stage, the implications of our results for interpretation of microwave backscattering from ocean waves are that specular reflection at small incidence angles such as 20° may be much more important than generally expected and that the relative frequency of occurrence of specular facets, sharp crests and capillaries or similar rough patches will determine the character of ocean scattering, both both incidence angle and frequency selection and for determination of modulation transfer functions.

I. INTRODUCTION

During the past ten years, the "composite model" has become increasingly accepted as the correct theory for the description of microwave scattering from the ocean surface. The basic premise of the theory is that microwave radiation (at moderate to large incidence angles) backscatters from "slightly rough" patches which are created by wind on the ocean surface. These patches are geometrically tilted by the underlying gravity waves and they also interact dynamically with the wind, the wind drift layer and the orbital current of underlying gravity waves. The electromagnetic theory that describes the scattering mechanism was developed by Rice[1]. The microwave radiation is assumed to scatter selectively from a Fourier component of the "slightly rough" surface which satisfies the Bragg condition. The theory that describes the interaction between this Bragg component and other wave components and currents and wind has gone through various stages of development to reach its present rather elaborate form as described by Hasselmann[2] and Wright et al.[3]

Despite this extensive theoretical development, there remain inexplicable observations in the field or laboratory which seem to suggest that the composite model may be inadequate or incomplete. Some examples are

(i) Polarization ratio -- The fact that Rice's theory correctly predicts a ratio not equal to unity has been one of the main reasons for the ready acceptance of Bragg resonant scattering as the dominant mechanism for microwave backscattering. However, the ratio has been much closer to unity than expected, especially for microwave wavelengths $\lesssim$ 3 cm and for large incidence angles[4]. The tilting introduced by the

composite model to explain the small ratio would require abnormally large surface slopes for the underlying long gravity wave.

(ii) Laboratory observations of the Doppler spectrum by Wright seem to require "a free wave system and two types of bound scatterers, one akin to a parasitic capillary wave and the other associated with wave-breaking"[5]. This goes beyond the surface conditions assumed and modeled in the theory. The width of the Doppler spectrum seems greater than expected from theory and the asymmetry of the spectrum is also unexpected[6].

(iii) Most people believe that Wright has conclusively proven in the laboratory that microwave backscattering is Bragg resonance scattering. As Wright put it, "proportionality between the scattered electromagnetic field and the Bragg wave amplitude is very nearly tautological for sufficiently small waves although an experimental verification has been given by Wright (1966)."[7] However, what Wright has shown is only that for a carefully generated sinusoidal wave with the Bragg wavelength, backscattered power is indeed proportional to the power of the Bragg wave[8]. What has yet to be demonstrated directly is that for a realistic random wave field with "slightly rough" patches on top of gravity waves, the backscattered power is proportional to the power of the appropriate "Bragg" Fourier component in the rough patch and nothing else. Later experiments in the field and laboratory by other investigators also fail to compare the absolute backscattered power with the power of the "Bragg component" because of the difficulty of calibrating radar systems absolutely and the obvious difficulty of quantitatively measuring the surface to the high degree of detail required for such a comparison.

(iv) Modulation theory -- Since the composite model gives no detailed description of how the Bragg waves interact hydrodynamically with the background waves, wind, currents, and other wave components, it does not explain how microwave backscatter from the ocean surface is modulated. Wright et al. proposed a theory of such interactions in an effort to explain modulations. So far, this theory appears to be having difficulty explaining the amount of modulation and the phase of modulation[8]. The success of any modulation theory will be contingent upon correct identification of the dominant sources of backscattering on the surface so that the modulation of such sources by background waves, currents, etc., can be correctly modeled.

We also cite here some miscellaneous observations which may not be widely known but which are worth considering and may also point to the need for a more complete scattering theory.

(i) Field observations by some Russian investigators that vv and hh backscattering are uncorrelated[9].

(ii) Differential Doppler -- Measurements of differential Doppler effects are completely unexpected on the basis of the composite model. There have been different conjectures on these effects and their implications but the entire subject remains an open question[10].

(iii) Field observations that breaking waves seem to generate large signals[11].

In summary, we find that in terms of absolute power, relative power (polarization ratio), and properties of the Doppler spectrum, comparison between the composite model and experimental measurements has been either unavailable or only qualitatively correct.

When we started this investigation of microwave scattering from water waves, it seemed quite unsatisfactory to us that despite the widespread conviction that "Bragg waves" are doing the scattering, there was no clear concept of what the "Bragg waves" actually are. Are they really corrugation-like wavelets or ripples on a windblown surface, or are they a Fourier component in a random rough patch? Or could they be a Fourier component of a fairly sharp crest? To answer these questions, the obvious thing to do would be to examine a scattering surface in great detail and see what it is actually like when scattering is taking place. We think that other investigators have chosen to bypass thi_ approach because

(i) The traditional approach to measurement of scattering is to average the signal over time and/or space.

(ii) It has been widely accepted that the ocean surface is highly random and is most appropriately described in terms of power spectrum with little or no correlation between the components. The adequacy of these assumptions about wave dynamics is now being questioned, especially for narrow-band spectra and/or steep waves. Whether or not they are adequate, a statistical approach has apparently been deemed necessary by others because a statistical description was the ultimate goal.

(iii) There is obvious difficulty presented by the need to measure the high frequency, small amplitude content on top of large background waves, i.e., the problems associated with the requirements of high frequency measurements with good spatial resolution over a large dynamic range. What is more, the measurement must be co-located, simultaneou and noninterfering with the microwave measurement.

(iv) The conviction that the composite model provides a good description renders further investigation of the role of "Bragg waves" as scattering sources on the surface quite unnecessary.

Our experience in the study of dynamics of deep-water waves encouraged us to consider the usefulness and feasibility of a deterministic approach. Initial studies further convinced us that it is both warranted and feasible to perform quantitative and deterministic water wave and microwave measurements to identify the relative contributions of specific surface features to total backscattering. More specifically, we attempted to measure the exact surface profile while microwave scattering is taking place. We focused our attention on short gravity waves generated by a wave paddle rather than on wind waves. The wave paddle generated waves are less random, more long-crested and yet exhibit certain characteristics similar to wind waves. They are therefore a logical first step for a deterministic study. With the wave profiles measured, we solved for the scattering by a numerical method and compared the computed results with the measured results. Using numerical modeling, we identified scattering contributions of different surface features. The experimental setup and procedures, numerical procedure, and final results are discussed in greater detail in the following sections.

II. EXPERIMENTAL FACILITIES AND EQUIPMENT

The experiment was performed in a wave tank which is 12 m long and 92 cm wide. The tank is filled to a depth of 90 cm with distilled water which is deionized almost continuously and whose surface is skimmed before every run. There is an open-circuit wind tunnel with a cross section of 122 cm x 92 cm on top of the wave tank (Figure 1). The inside surface of the wind tunnel is completely covered with 40 db microwave absorbing material. For the purpose of this experiment, the wind tunnel serves only the purpose of an anechoic chamber. Water waves are generated by a wave paddle at one end of the tank and propagate to the other end where they are absorbed by a shallow-angle beach. The wave paddle is programmable, but for the purpose of this experiment, it is set at a fixed frequency of 2.5 Hz, producing waves roughly 1 cm in amplitude, corresponding to $ka \sim 0.17$ (where k is the wavenumber and a is the wave amplitude or half the peak to trough height). The wave tank-wind tunnel is described in detail by Lee[13].

The x-band radar system is shown in Figure 2. It is a 9.23 GHz (3.248 cm) cw superheterodyne coherent system with 30 MHz IF, roughly 100 mW transmitted power and dual transmitting and receiving channels, each of which provides individual phase and amplitude (i.e., linear detection) outputs. (Only one of the two channels is shown in Figure 2.) Each of the channels can be roughly "nulled" by an E-H tuner and finely "nulled" with a static balancing bridge which is a combination of variable attenuators and phase shifters. The nulling provides for the cancellation of the background stray reflections. The antenna is a corrugated, conical horn with a half angle of 16° and a 22.9 cm aperture fitted with a matched

dielectric lens with a focal length of 45.7 cm. The choice of the corrugated conical horn, sometimes known as the scalar feed, is necessitated by the requirement of dual-polarization. It provides an antenna pattern almost independent of polarization. Furthermore, there is little cross-polarization between perpendicular polarization states. It also has much lower sidelobes than rectangular or pyramidal horns. In short, it is almost the ideal antenna. The need for focusing the radar is based on two requirements. For unambiguous intepretation of results, we want to illuminate a small enough area so that at most one water wave is illuminated at a time. Secondly, we want to have plane wave illumination even though placing the horn inside the wind tunnel puts the water surface within the near-zone of the horn. Both requirements are met by focusing. Even though the corrugated horn has minimal sidelobes, the addition of a lens introduces reflections at the lens-air interfaces which increase the sidelobe levels. The additional sidelobe level was found to be quite detrimental to our measurements where accuracy of absolute power is required. Matching of the dielectric lens overcomes this problem and is found to be a necessity. Details for the design of the horn can be found in Love[14]. The technique of matching the lens to reduce reflections from the lens surface can be found in Morita, et al.[15] Wave guides of the two separate channels are connected to the horn via an orthomode transducer which provides 40 db isolation between channels and establishes the two perpendicular polarizations. The horn and the orthomode transducer are adjusted so that the two polarizations are respectively vertical and horizontal. The combination of the corrugated horn and the matched lens and the orthomode transducer produces a 3-db beamwidth of 8.48 cm and 8.43 cm for vv and hh polarization respectively at the 45.7 cm focal plane along the horizontal

axis. Cross polarization (vertically transmitted, horizontally received) is down by 36 db along the vertical axis and down by 30 db off the principal axes. Phase variation within the 3 db beamwidth is less than 28°.

To measure an almost instantaneous profile of the water surface while microwave scattering is taking place, we have developed a scanning laser slope gauge (SLSG) which is a natural extension of the laser slope gauge first developed by Chang, et al.[16] We will discuss only the principal features of the SLSG here as its details will be presented elsewhere[17]. We first review here the working principle of the laser slope gauge. With a laser beam vertically incident on the water surface, the angle of the refracted beam is almost directly proportional to the water slope under the laser illumination. If the angular displacement can be converted by a lens into a linear displacement and then detected with an optical linear displacement sensor, the output of the displacement sensor will be an indication of the water slope. Since the laser typically has a spot size of 0.5 mm, the laser slope gauge has spatial resolution much better than a conventional capacitance level gauge. The frequency response of the slope gauge will be limited by that of the linear displacement sensor, which typically has a response of several thousand Hz, high enough for water wave measurement. In the original design of the slope gauge by Chang, et al., the laser beam is incident from above the water, bent around under the water and detected by a detector above the water. Since the detector interferes with the microwave measurement, we modified the design so that the laser beam is still incident from above, but now the optical elements for reception are 25 cm below the water surface and the linear displacement sensor itself is placed outside the wave tank, viewing the optical elements through the plate glass which forms the side of the wave

tank (see Figure 3). With this arrangement, the laser slope gauge provides a noninterfering, co-located simultaneous measurement of the surface with good spatial resolution and frequency response. One difficulty quickly becomes apparent, however, when we try to correlate what is observed by the slope gauge with what is observed by the radar. The slope gauge observes what is happening at one point whereas the microwave is observing a large area. To remedy the situation, we implemented scanning of the laser beam so that it scans the water surface over 13.3 cm at 39.063 Hz. The detected output thus provides an almost instantaneous slope profile of the surface at close to 40 times/sec. The angular range of the SLSG is about 60° which can be offset in either direction. With calibration, the slope gauge has an accuracy of ±0.3°, so that it can be meaningfully integrated to provide the displacement profile. In summary, the SLSG is almost the ideal instrument for surface measurement, its only defect being that it scans along just one dimension.

Besides the SLSG, another optical sensor was deployed to monitor the presence of specular facets at an angle normal to the microwave incidence on the water surface. This is accomplished by putting a projector lamp to one side of the corrugated horn and a camera with a 70-200 mm zoom lens to the other side. Both the projector lamp and the zoom lens are aimed at the patch of surface under microwave illumination and both are set at roughly the same angle as the horn. Fine adjustment is achieved by putting a small mirror with the correct angle at the center of microwave illumination. The camera is then adjusted to intercept light from the projector lamp. A large circular photodiode detector 2.5 cm dia. is placed at the film plane of the camera whose shutter is left open. After amplification, the output of the detector shows spikes whenever specular facets appear in the field of view of the

camera. This is our criterion for separating the "nonspecular" from the "specular" scattering events. Since the sensor of the SLSG is light sensitive, a green filter is put in front of the projector lamp and a red filter in front of the linear displacement sensor. This arrangement was found to be satisfactory for the SLSG.

For comparison purposes, a capacitance level gauge was installed close to the side of the wave tank, just 45 cm cross-tank from the center of the microwave antenna pattern, but shielded from it by a sheet of microwave absorbing material.

The x-band radar is used in conjunction with the three surface diagnostic instruments (the SLSG, the optical specular reflection sensor, the capacitance level gauge) to study nonspecular microwave backscattering events. The amplitude output of the vertical and horizontal polarizations, phase output of the vertical polarizations and output of the SLSG were captured simultaneously on four separate channels of a digital oscilloscope and then recorded on floppy discs. The same microwave amplitude and phase outputs, together with outputs of the specular reflection sensor and the capacitance level gauge were recorded on a strip chart recorder. The specular reflection sensor output was used to screen out the specular events. The nonspecular events were then analyzed by a Prime 750 minicomputer.

The specular events are not susceptible to computer analysis. This is because the SLSG scanned profile is not a good representation of the event as the specular facets are distributed across the wave front and may or may not be intercepted by the laser beam. It was therefore decided that the best way to investigate the "specular" events is by photography. We replaced the projector lamp with photographic flash units and used photographic film in place

of the photodiode detector in the camera. Either one or two flashes were used. In the single flash model, the room lighting is turned off and then the camera shutter opened. The flash unit is triggered by a threshold detector detecting the microwave vertical polarization amplitude exceeding a certain preset level. The exact instant the picture is taken is recorded by a photodiode sensing the flash which typically lasts 2 msec. In the double flash mode, the second flash is triggered to go off after the first one after a preset time delay.

III. EXPERIMENTAL PROCEDURE

The corrugated horn is set up at a fetch of 8.4 m looking uptank. The incidence angle can be varied between 40° and 70°. For this experiment, data were taken at 40°, 55°, and 67.7°. After proper alignment of the scanning laser beam and the microwave horn so that they both roughly illuminate the same area, the antenna patterns are measured at the water surface and at 1 cm above the water surface. This is done by lowering the water level by roughly 22 cm and then floating a tray on the water and covering it with a large sheet of 40 db microwave absorber. This, together with the microwave absorber-covered wind tunnel, provides a minimal level of stray background. The radar unit is fine tuned to null away this background. A metal sphere of 0.952 cm O.D. is then hung from a traverse and moved horizontally in the uptank direction through the antenna beam at the height of the original water level. The two receiving channels of the radar unit are adjusted to have the same outputs. The microwave outputs are then recorded as the antenna patterns at "water level". The sphere is raised 1 cm and the procedure repeated to record the antenna patterns at 1 cm above water level. The recorded amplitude patterns become part of the input to the computer for numerical computation. The recorded phase channel gives the effective microwave incidence angle at the water surface. This effective angle is the one used in computations. After this calibration, the water is raised to its original level and its surface skimmed for at least 2 hours to ensure a clean surface. Water waves are then generated by the wave paddle at 2.5 Hz and with roughly 1 cm amplitude. Outputs from the capacitance gauge, the specular reflection sensor, and the amplitude channels of both vv and hh polarizations are recorded continuously on a strip chart recorder. Outputs of the vv and hh amplitude

channels, vv phase channel and the SLSG are captured on the digital scope on an event by event basis, each one being triggered by the vv channel crossing a preset-threshold which is roughly 20 db below the maximum observed, so that the captured events span roughly a 20 db range. The sampling time on the digital scope is set at 200 μsec and there are 1024 points per recorded event. By comparison, a typical burst lasts 0.2 to 0.3 sec. At a scanning frequency of 39.063 Hz, there are 128 points per scan and 8 scans per event. After an event is captured, the specular reflection sensor output on the strip chart is checked to see if there are spikes indicating the presence of specular facets. If the spikes are absent, the event is deemed a "nonspecular" event and recorded onto a floppy disk. Some of the "specular" events are also recorded for comparison purposes. Roughly 100 events are recorded per incidence angle. After each run, we screen the recorded events to reject the obviously bad ones. Of the remaining good events, about 40 events/incidence angle are then transferred to a Prime 750 computer for analysis.

For the investigation of specular events, the projector lamp for the specular reflection sensor is replaced by photographic flash units while ASA 400 black and white film is put into the camera which is set at f-8 to f-11. In the single flash mode, the camera shutter is opened and a single flash unit is set to be triggered when the microwave vv channel amplitude crosses a preset threshold, which is usually a very high level where specular events are more likely. In the double flash mode, the second flash unit is triggered after the first after a preset time delay of either 10, 20, or 30 msec. The exact instant(s) when the flash (or flashes) goes off is sensed by a photodiode. Outputs of radar and photodiode are captured on the digital

scope and recorded on chart paper. The single flash mode produces pictures which display the specular facets. The double flash mode shows how far the facets have moved in between the flashes. The velocity measured can then be compared with the Doppler shift measured by the radar.

IV. NUMERICAL PROCEDURE

For the analysis of the "nonspecular" events, we use the Method of Moments to numerically compute the backscattering amplitude and phase from a measured profile and then compare them with the measured values. The Method of Moments numerically solves for the exact electric surface current from the integral equation of scattering and then computes the scattered field. There are no restrictions on the curvature of the surface. The length of surface that can be computed is limited by the computer's matrix handling capacity and speed. For example, using 15 points/microwave wavelength and a surface length of 15 microwave wavelengths, the machine must solve a roughly 200 x 200 matrix equation. For the Prime 750 minicomputer, this takes typically 10 minutes for either polarization. The computing time goes up roughly as the cube of the dimension of the matrix so that the limitation of computing time is quite obvious.

A complete exposition of the Method of Moments can be found in Ref. 18. Based on the method, Lentz[19] has written computer programs for both vv and hh polarizations which we found to be easily adapted to our computer. We will discuss here briefly the formalism to illustrate the conventions used. We will also show where modifications of Lentz's programs are made.

For an incident wave with horizontal polarization (E-field along the $\hat{z}$ direction, see Figure 4), the magnetic field is transverse (transverse magnetic polarization, or TM mode). The boundary condition is

$$\vec{E}^i + \vec{E}^s = 0 \tag{1}$$

where $\vec{E}^i$ is the incident E-field and $\vec{E}^s$ the scattered E-field. The scattered field is given in terms of the $\hat{z}$-directed surface currents $J_z(\vec{\rho}')$ by[19]:

$$E_z^s(\vec{\rho}) = -\frac{k\eta}{4}\int_c J_z(\vec{\rho}')H_0^{(2)}(k|\vec{\rho} - \vec{\rho}'|)d\ell' \qquad (2)$$

for the two dimensional case, where $\vec{\rho}$ is the observation point, $\vec{\rho}'$ is a point on the surface and $H_0^{(2)}$ is the Hankel function of the second kind and order zero, η is the impedance of free space, k is the wavenumber $2\pi/\lambda_e$, λ_e is the microwave wavelength, c is the contour and ℓ' is distance along the contour. Combining this with the boundary condition gives the integral equation for the surface current in terms of the incident $\vec{E}^i$ field:

$$E_z^i(\vec{\rho}) = \frac{k\eta}{4}\int_c J_z(\vec{\rho}')H_0^{(2)}(k|\vec{\rho} - \vec{\rho}'|)d\ell'. \qquad (3)$$

To avoid edge effects in computation over a finite range, Lentz used an antenna illumination pattern which is constant throughout most of the range, but tapers off to zero before it reaches both edges. The integral in the integral equation then has a finite range and by "point-matching" the integral equation is transformed into a finite-dimensional matrix equation which can be solved by a computer. The formulation for vertical polarization (transverse-electric polarization, or TE mode) is similar and just slightly more complicated. Having solved for the surface currents, the scattered fields can be calculated by integrating eq.(2). For both TE and TM modes, the computed and plotted values are the values normalized with respect to distance from the scattering surface, i.e.,

$$\text{for TM mode} \qquad H_{zc}^s = H_z^s(\vec{\rho})\sqrt{|\vec{\rho}|}\, e^{jk|\vec{\rho}|}$$

$$\text{for TE mode} \qquad E_{zc}^s = E_z^s(\vec{\rho})\sqrt{|\vec{\rho}|}\, e^{jk|\vec{\rho}|}$$

where H^s_{zc}, E^s_{zc} are the computed and plotted values, and $H^s_z(\vec{\rho})$ and $E^s_z(\vec{\rho})$ are the true scattered fields at $\vec{\rho}$.

For any given incidence angle, Lentz's programs require as inputs the antenna pattern and a surface displacement profile. Our SLSG has a scanning range of 13.3 cm or roughly $4\lambda_e$, which is just over half the water wave wavelength of 25 cm (or $7.7\lambda_e$). For a description of the high frequency features of the surface, this scanning range is quite adequate as the capillary waves have a typical extent of 6 cm or less, which in this case corresponds to about $2\lambda_e$, and the crest region where the slope changes drastically has an extent of 1.5 cm or less, here corresponding to $1/2\lambda_e$. For computation, however, the small range creates two artificial edges which produce strong interference with the true scattering. We therefore extend the computation range to $15\lambda_e$ ($x = -7.5\lambda_e$ to $x = +7.5\lambda_e$). The scanned range is roughly between $x = -2\lambda_e$ to $+2\lambda_e$. The regions between $x = -7.5\lambda_e$ and $-2\lambda_e$ and $x = +2\lambda_e$ and $+7.5\lambda_e$ are filled with exponential tails which are made to match smoothly the measured slopes at $x = -2\lambda_e$ and $x = +2\lambda_e$, respectively. During the scan measurement, the water wave has moved. The measured slope profile therefore has to be "contracted" to arrive at the correct instantaneous slope profile. This correction is made by assuming the whole water wave moves at the phase velocity of a 2.5 Hz wave, i.e., 62.6 cm/sec. The resultant contraction is about 9%. Any component of the wave moving at a slightly different velocity will introduce an error which will be a small fraction of the 9%, i.e., a very small error. The slope profile is then integrated by 5-point Gaussian quadrature to provide the displacement profile as required by Lentz's program.

Even with the extended range for computation, the antenna pattern strengths at $x = +7.5$ are still significant, especially for large incidence

angles such as 70°. We therefore modify the antenna patterns to make them taper off faster toward the edges at $x = \pm 7.5$. If our assumption is correct, that only the region around the crest (more specifically $x = -2\lambda_e$ to $x = +2\lambda_e$) contributes significantly to backscattering, then any model antenna pattern can be used so long as it approximates the true pattern between $x = \pm 2\lambda_e$ and is "smooth" enough and tapers off fast enough. We have one particular realization in which the model approximates the true pattern by 2 quadratic functions near the center and tapers off as Gaussians towards the edges. This model antenna pattern is the two-way antenna pattern. The one-way pattern, i.e., the incident field on the water surface, is given by the square root of the two-way pattern.

With the extended surface profile and the incident field prescribed, we choose a grid density of 15 points/λ_e in applying Lentz's program. In the final step when the surface currents are integrated again to give the scattered field, the one-way antenna pattern is again applied. This provides a scattered field which is strictly speaking correct only for our particular antenna and for the backscattering direction.

With the extended range of computation and a tapered antenna pattern, the edge effect of computation still shows up in some cases, especially in TE mode and for large incidence angles. This is most evident when the scattered power is plotted as a function of scattering angle. An oscillation will be seen as a function of angle and the angular period of the oscillation can be shown to be due to the pair of computational edges. To eliminate this edge effect, we first carry out the original computation with a computational range of $+7.5\lambda_e$ to $-7.5\lambda_e$. We then extend the range by a half Bragg wavelength

in both directions and compute again. The complex amplitudes of both computations are then added together to eliminate the amplitude due to the edges. This doubles the computation time. Consequently, we use this only in the TE mode for 40°, 55°, 70° and for the TM mode at 70°. Test cases at 40° and 55° for the TM mode show that the double computation is not required.

For the analysis of absolute backscattered amplitude and polarization ratio, one scan per event is chosen and analyzed for both vv and hh polarizations using Lentz's programs with the above procedure. The average powers of both polarizations during the scan time are also measured. A comparison of measured power vs. computed power in both polarizations can then be made. The comparison is however only relative. It must be remembered that the computed power is that for a two-dimensional wave whereas the measured power is that for a wave which is far from being truly two-dimensional, especially when it is in the stage of breaking. Furthermore, the antenna pattern also has a finite extent in the cross-tank direction. It is difficult to determine accurately the error due to the combined effect of these two factors. Rather than trying to estimate the error, we performed a calibration with known two-dimensional targets. Cylinders and wedges with widths close to that of the wave tank were used. The metallic cylinders have o.d. of 0.3175, 0.2381, and 0.1558 cm, and lengths of 91.5 cm. The wedges used have 160° and 140° inclusive angles and widths of 91.5 cm. The backscattering from these standard targets is then measured. For the cylinders whose radii are $\ll \lambda_e$, the computed backscattered power (normalized with respect to distance) can be obtained by series expansion. For the wedges, the computed power (again normalized with respect to distance) is obtained from GTD. The measured backscattered power vs. computed power for these two-dimensional targets is plotted and the

best fit line through the points constitute our "absolute calibration". With the "absolute calibration" line, an absolute comparison between measured power vs. computed power, which has never before been attempted, can now be made. A similar comparison is also made of the measured polarization ratio vs. computed polarization ratio.

For the analysis of phase or Doppler shift, three successive scans/event for certain selected events are chosen. The phase for each scan is calculated by using Lentz's programs. The change of phase from one scan to the next is due to both the movement of the wave form and also the change in shape of the wave form. The calculated change of phase can be compared with the measured Doppler shift for the selected events.

Initially, the analysis centered on comparing the microwave measurements with numerically computed results using as inputs the SLSG measured profiles. This validates both our measurement procedure and numerical procedure and demonstrates the feasibility of the deterministic approach. It does not identify which features of a short gravity wave are the dominant sources of microwave backscattering or their relative strengths. We know from preliminary qualitative observations that microwave backscattering from mechanically generated short gravity waves is associated with wave breaking. During breaking, the wave crest attains a very small radius of curvature and capillary waves are formed on the front side of the wave. A turbulent wake may or may not be formed on the back side, depending on how violent the breaking is. We then sought to determine which of these surface features scatters microwave radiation and their relative importance as scattering sources. Since the turbulent wake is fairly random in two dimensions, the profile generated by the SLSG in one dimension will not be a good representation in such a case. Also, the occurrence of the turbulent wake is sufficiently rare, and when it occurs is usually

sufficiently weak, that we will focus our attention only on the "gentle breaking" events in which only the small radius crest and the capillary waves are present. In such cases, we can perform a "numerical experiment" in which an actual wave profile is replaced by one in which the capillary waves have been smoothed away. We call such a model the background wave form. Scattering from the background wave form can again be computed using Lentz's programs. Since the difference between the background wave form and the original wave profile is only a small perturbation, the difference between the scattering amplitude of the background wave form and that of the original wave profile can be ascribed to be the scattering amplitudes of the perturbation, i.e., the capillary waves. This can be checked directly by putting the capillary waves on an inclined plane with the appropriate slope and numerically computing the scattering amplitudes again. The question naturally arises as to whether the scattering from the capillary waves is describable by small perturbation theory. To this end, Barrick's analysis of small perturbation theory[23] has been extended for a deterministic surface (see Appendix B). Within the same computation range of $\pm 7.5\lambda_e$, given a surface profile, small perturbation theory prediction of the scattering can be compared with that of numerical integration. The background wave form resembles a rounded wedge around the crest region. Numerical computation of scattering from the background wave form is compared with that from a sharp wedge and also from wedges with varying degrees of rounded tips. The sharp wedge computations are in turn compared with GTD predictions. We find that the roundedness of a wedge is simply a small perturbation from a sharp wedge so that the effect of roundedness on scattering can be estimated from small perturbation theory. In this manner, we have decomposed the microwave scattering from a realistic water wave into its most fundamental components.

V. RESULTS AND ANALYSIS

A. Qualitative Results

In the following, we present first some of the qualitative results we obtained in a preliminary study, which point to the need for a more quantitative study, and then results of the quantitative study. Figure 5 shows a typical recording of backscattering at 55°. The top trace is the output of a stationary laser slope gauge (laser beam stationary and not scanning). The second trace is the output of a capacitance level gauge. The self modulation of the water wave is evident. One out of every 3 or 4 waves attains a small enough radius of curvature to break and generate capillary waves on the front side. The capillary waves are highly pronounced in the slope recording, and hardly noticeable in the capacitance gauge output, showing that the laser slope gauge is intrinsically a better instrument for recording high frequency surface features. The capillary waves typically have a frequency over 100 Hz, sometimes as high as 360 Hz. The third and fourth traces are the amplitudes of the backscattering in vertical and horizontal polarizations. The fifth trace is the phase of the backscatter in vertical polarization. We note immediately that

(i) scattering occurs in discrete bursts which are highly correlated with the breaking events. The discreteness of the bursts is a result of both the fact that the microwave beam is focused and the fact that the wind tunnel has been carefully shielded to minimize background reflection. This discreteness is probably contrary to the general notion that microwave scattering is noise-like, in which case a statistical analysis would seem to be the only logical approach.

(ii) The occurrence of a microwave burst is either coincident or slightly ahead in time of the corresponding capillary wave packet [e.g., events (a) and (d) in Fig. 5].

(iii) Some microwave bursts are not accompanied by any capillary waves, in which case the microwave burst occurs behind (in time) a corresponding wave which usually appears as a sharp peak in the slope channel [e.g., event (c) in Fig. 5].

(iv) "Old" capillaries are usually accompanied by no burst at all, or only a very small one [e.g., events (b) and (d) in Fig. 5].

These observations seem very paradoxical at first. Observations (ii) and (iii) seem to suggest that microwave bursts are associated directly with the capillary waves. If a wave should break before it reaches the laser beam (which is in the center of the antenna pattern), the microwave return should show a burst before the laser beam sees the capillary, and hence observation (ii). If a wave should break after it passes the laser beam, the laser beam will see only a sharp peaked wave and no capillary waves whereas the microwave return should show a burst slightly behind the peaked wave, and hence observation (iii). However, observation (iv) seems to suggest that capillary waves are not the microwave scatterers per se. Furthermore, capillary waves with a frequency of $\sim$ 100 Hz and wavelength typically $\leq$ 5 mm also fail to meet the "Bragg" scattering frequency or wavelength criterion. One way to determine whether the microwave bursts are associated directly with the capillary waves is to examine whether there is any significant scattering prior to wave breaking (i.e., before capillary waves are created), which is an event sharply defined in time. With a stationary slope gauge, it takes a series of careful time measurements to show that scattering starts slightly before breaking has

occurred. With a SLSG, this conclusion is easily verified. This suggests that microwave scattering can occurr even when the surface is macroscopically smooth, contrary to the common notion that it has to be "slightly rough" in order to backscatter at moderate to large incidence angles. Before a wave breaks, the only high frequency feature on the wave is the small radius crest. We are thus prompted to examine existing theories which consider scattering from such a surface feature. It can be seen that the small radius crest (typically with radius < 1 cm, or $<< \lambda_e$) is not describable by physical optics, which requires large radius of curvature for its tangent plane approximation. Nor is the small radius crest describable by Rice's small perturbation theory which allows small radius but not large amplitude. The small radius crest is therefore outside the realm of applicability of the two components that constitute the composite model. This observation leads one to ask why the existence of such small radius features has not been considered in the development of the composite model. In addressing this question, it must be remembered that during the 1960's when the composite model was first formulated, the widely accepted interpretation of ocean waves was that they are linear superpositions of uncorrelated dispersive components which are most aptly described in terms of a power spectrum. If all these assumptions are valid and if we assume the spectrum varies roughly as k^{-4}, then it can be shown[20] that there is a natural wavenumber below which the long wave components can be considered to constitute a long wavelength undulating background with radius of curvature that is large everywhere, thus satisfying the requirement of physical optics. The components having a wavenumber smaller than the critical wavenumber together constitute a

small perturbation with small amplitude everywhere, thus satisfying the requirements of small perturbation theory. Under these conditions, the composite model is therefore not only attractive on the basis of electromagnetic considerations (as it forges a union of physical optics and small perturbation theory) but it can be justified based on hydrodynamic considerations. Recent studies of water wave dynamics have shown, however, that deep water waves may have significant nonlinear effects, including components which are both correlated and nondispersive, so that the assumptions on which the composite model is based do not always apply. These nonlinear characteristics of finite amplitude deep-water waves can be exhibited in their simplest form in the laboratory by generating a uniform wave train with a wave paddle and no wind and observing its evolution as it propagates down a wave tank. In our laboratory when we generate such a wave train with wavelength of 25 cm and amplitude of 1 cm (i.e., ka = 0.17), the self-modulation of the wave is sufficiently strong by the time they have propagated 6 m down the tank that individual waves have small radius crests and undergo breaking. In such wave systems, small radius crests are important features which must be taken into consideration in accounting for microwave backscatter. Although backscattering from such features cannot be described using the composite model, there is an electromagnetic theory available [(Keller's Geometry Theory of Diffraction (GTD)][21] that should provide a good description.

Briefly, GTD assumes that the diffraction coefficient of a wedge is derived from an asymptotic expression of the rigorous solution for the wedge, which is available. The description of wedge diffraction by GTD results in simple expressions that are easy to evaluate. Furthermore, it is polarization dependent. The polarization ratio for a wave-like wedge (wedge with front and back slopes equal to typical values for a short gravity wave) is roughly between 6 to 10 db at 55° incidence angle, a figure with the same order of magnitude as

that measured for the ocean. The ratio goes to 0 db as the wedge angle decreases (and we know that the polarization ratio measured for the ocean goes to 0 db as the sea roughens). Finally, we know from our laboratory measurements that the radius of curvature of the crests of the short gravity waves in the stage just before breaking can be typically $\leq$ 1 cm, and as small as 3 mm. This is much smaller than λ_e, i.e., the crest is approximately a sharp edge relative to λ_e so that applying the wedge diffraction theory of GTD should provide a reasonable description of the scattering. Although the wedge diffraction theory of GTD appears to be appropriate for this problem, we have also considered the possibility that wedge diffraction as described by GTD might be equally well described by small perturbation theory in terms of the Bragg Fourier components of the wedge. In doing so, we noticed that a "small amplitude" wedge (large inclusive wedge angle, small slopes and amplitude) satisfies all the criteria for Rice's small perturbation theory, which requires small amplitude but remains valid even as the radius of curvature of the corner of the wedge becomes vanishingly small. It also naturally satisfies the criteria of Keller's GTD, which is valid for all wedge angles. Rice's small perturbation theory should thus be applicable to a small amplitude wedge and should give the same result as that of GTD for a small amplitude wedge. In Appendix 1 we show that the two theories do agree for such conditions. Furthermore, we show there that the scattering coefficients predicted by the two theories start to diverge as the wedge amplitude increases. As GTD is valid for all wedge angles, this indicates that small perturbation theory is increasingly in error as wedge angle decreases, i.e., the backscattered power is no longer linearly proportional to the power of the resonant Fourier component of the surface, which is really not so surprising. It simply implies that with the perturbation approach, higher and higher order approximations are required as the wedge angle decreases and wedge amplitude increases.

At this point, it might be tempting to propose that for microwave scattering purposes the ocean be modeled using wedges in addition to wind generated ripples (noting also that the wedge has a power spectrum of k^{-4}). However, the SLSG shows that short gravity waves near breaking are at best modified wedges because the tips are rounded and the front and back slopes are not straight but are slightly concave. Furthermore, the role of specular reflection and the contributions to scattering from the capillary waves and turbulent wakes are uncertain but potentially significant. Modeling short gravity wave scattering simply as wedge diffraction will therefore result in a semiquantitative theory at best. It is for this reason that we decided to investigate the problem of scattering from such waves in great detail to isolate and identify quantitatively the contributions of the different scattering processes.

B. Quantitative Results

The above describes the rationale for our deterministic study of backscattering from short gravity waves. In the following we present the results of that study. Figure 6 shows a typical strip chart recording at 67.7°. Event A is a typical "specular" event in which the specular reflection sensor shows spikes while the amplitudes at the two polarizations are nearly equal. Event B is a typical "nonspecular" event in which the specular sensor is devoid of spikes and the vv channel has a noticeably larger amplitude than hh. Event B is recorded on the digital scope whose display is shown in Figure 7. Notice that the time scale is now much more expanded than the strip chart. The SLSG channel shows the wave beginning to break in the first scan. Between scan 3 and scan 7, the parasitic capillaries become fully developed as they move across the scan range. The vv and hh amplitude channels are duplicates of those on the strip chart, though in greater detail. The vv phase channel shows

how the backscattered vv channel phase is varying in time. It jumps discontinuously for every 360° change. The number of cycles/sec gives the Doppler shift. Scan 4 in Figure 7 is the scan chosen for computer analysis for this event. The upper trace in Figure 8(a) shows the SLSG output with exponential tails added on both sides to fill the computation range. The lower trace of Figure 8(a) shows the integrated displacement profile of the water wave. Figure 8(b) shows the resultant vv and hh scattered power as a function of scattering angle. (See Figure 4 for definition of scattering angle.) As we have mentioned, only the power at 22.3° (corresponding to backscattering for 67.7° incidence angle) is strictly correct because of the antenna pattern we have applied. Roughly 40 events for each of the incidence angles 40°, 55°, 67.7° have been computed in this manner. The computed power is plotted vs. the measured power for the different incidence angles in Figure 9. The solid line in the figure is the "absolute calibration" line which was described earlier. If water waves are "long-crested" enough that they are uniform across the antenna beam width, and if measurement and numerical procedures are both correct, then the points of measured power vs. computed power should fall on the calibration line. The measurement procedure for water wave backscattering is the same as that for the standard targets. The numerical procedure used for computing the backscatter from the water waves is the Method of Moments, which has also been used to check the GTD result for wedges. It thus seems odd that the points of measured power vs. computed power for the water wave do not seem to fall around the calibration line. Although measured power does seem to be proportional to computed power over a range of almost 30 db, measured power appears to be about 4 db less than what it should be. We believe the explanation is that the water wave is not long crested enough to cover the width of the antenna pattern, which reduces the amount of scattering. The amount of scatter of the data points is about ±4 db about the best fit line.

This again is most probably due to the nonuniformity of the crest, so that the SLSG scanned profile is not representative of the average profile. To see whether cross-tank variation is significant, we used a beam splitter to split the scanning laser beam into two parallel scanning beams, each on being detected by its own sensor. We thus have simultaneous parallel scans about two inches apart. Cross-tank variation across the wave is observed to be not insignificant. To fully characterize a wave for comparison with microwave scattering predictions, a two-dimensional scan would seem the only solution. This however would require much more sophisticated instrumentation and the numerical computation would be prohibitive. A one-dimensional-scan deterministic study, despite these deficiencies, seems the only feasible approach at present.

Figure 10 shows the measured polarization ratio versus the computed polarization ratios for the different incidence angles. The measured values seem to be roughly proportional to, but diverging progressively from, the computed values as the incidence angle increases. Implicit in these computations, however, is the assumption that water is a perfect conductor. In fact, water is a dielectric and its dielectric constants at microwave frequency are known[22]. It would be difficult to compute numerically using a dielectric interface. Instead, we recall that in small perturbation theory, the difference between a perfect conductor and a dielectric appears in the evaluation of the constants α_{vv} and α_{hh}[24]. For 40°, 55° and 67.7° incidence angles, α_{vv}^2 is decreased by 2.597 db, 3.352 db and 4.300 db, respectively, and α_{hh}^2 is decreased by 1.548 db, 1.156 db and 0.756 db, respectively. When these first order corrections are added to our numerically computed results, the agreement between measured polarization ratio and computed polarization ratio is much better (Figure 11). Indeed, the original slight disagrement shows that our measurements and

numerical compuations are correct to the extent that even the fact that water is not a perfect conductor is noticeable. The dielectric corrections have been included in the plot of measured power vs. computed power (Figure 9).

Figure 12 shows how the computed phases compare with the measured phases for one event at a 55° incidence angle. The continuous line segments are the measured phases as a function of time. (The phase channel in Figure 7 shows a discontinuous jump of 360° every cycle. We have eliminated the jump so that the phase increases monotonically.) The squares represent the computed phases of three successive scans. The triangles are the phase representation of the location of the crest, i.e., if the crest were a line scatterer, the phase of backscattering from it as a function of time would be represented by triangles. Since phase is relative, we have put the computed phase and the phase of the crest of the middle scan right on the line of the measured phase. Usually, the measured phase goes up quite linearly with time. We show here one particular case in which the measured phase changes quite drastically during the course of three scans. It can be seen that the computed phase and the crest phase follow the measured result quite well. The rate of change of the phase is the Doppler shift. Since phases are computed for 3 scans, there are 2 computed Doppler shifts and 2 crest Doppler shifts per event. The two computed values per event are averaged and plotted versus the averaged measured values in Figure 13. This is also done for the crest Doppler shift in Figure 14. It can be seen that both averaged computed values and averaged crest values agree remarkably well with the average measured values. We may perhaps draw some conclusions from these observations: (i) The fact that all the average values agree so well means that on a time average over about 50 msec, the shape of the wave form is quite constant so that the crest has the same average

velocity as the wave form. (ii) The fact that agreement between calculated and measured phase results is better than between the calculated and measured amplitude and polarization results probably means that although cross-wave variation may affect the amplitude results, there is less cross-wave variation in velocity.

We have shown so far that in terms of absolute power, polarization ratio and Doppler shift, measured results agree quite well with computed results. This validates both our experimental and numerical procedures, so that we can proceed to use them to identify and analyze the relative contributions of various surface scattering sources to the overall backscatter. This is done by computing the backscattering from simplified forms of the actual measured wave form and comparing the results to the backscattering from the actual wave forms.

We first used simplified wave forms in which the capillary waves on a measured profile were smoothed away leaving only the background wave form. If we take the wave in Figure 8 as our example, then the smoothed background wave form with its computed scattering is shown in Figure 15. The difference between the original wave profile and the smoothed background wave form is the contribution to the wave form from the parasitic capillary waves. We put this on an inclined plane at an angle of 14.5°, which is roughly the average slope of the front face of the original wave on which the capillary waves were located. The resultant wave form, together with the computed scattering from it, is shown in Figure 16. The scattering is dominated in the forward direction (scattering angle $> 90°$) by specular reflection and specular reflection side lobes. To get a better idea of the scattering due to the capillaries alone, the scattering from the flat inclined plane at 14.5° is computed and subtracted from the scattering from the capillaries on the inclined plane. The result is

shown in Figure 17. (This involves subtraction of two complex amplitudes. The absolute magnitude of the result is displayed as power in db.) It can be seen that this difference can be accounted for very well by the scattering from the capillaries, especially in the backward direction. It is thus meaningful to think of scattering from the original wave as an algebraic sum of scattering from the background wave form and scattering from the capillaries. This is not unexpected as the capillaries are a small perturbation. Scattering from the capillaries on the inclined plane can also be estimated by small perturbation theory (see Appendix 2). The Fourier spectrum of the capillaries is shown in Figure 18(a) and the scattering predicted by SPT is shown in Figure 18(b). It can be seen that small perturbation theory explains the scattering from the capillaries nicely. Notice that Figure 18(b) looks like a mirror image of Figure 18(a). This is to be expected from SPT, which predicts that scattering at small scattering angles is due to spectral components at large K and vice versa. Thus the specular reflection at 120°-130° scattering angle corresponds to the K = 0 peak and the enhanced scattering around B,C and the dip around A can be fully understood in terms of the features b, c, and a in the Fourier spectrum of the capillaries. The most prominent oscillations in the capillary waves have a wavelength of about $0.2\lambda_e$ (5-6 mm), corresponding to the feature marked d around K = 70 on the Fourier spectrum. Backscattering around θ_i = 67.7° (scattering angle = 22.3°) however, is due to the feature C around K = 20-30. Thus the capillaries per se are not doing the scattering because they have the wrong wavelength. Rather, it is the roughness associated with them that is causing the scattering in a small perturbation manner. At higher microwave frequency, e.g., Ka band, at the same incidence angle of θ_i = 67.7°, the backscattering would be due to Fourier components around

K = 70-80. In this sense, the Ka-band microwave radiation is indeed scattering resonantly from the capillary waves, as shown in Figure 19. Notice that the backscattered power at 67.7° for the Ka band (λ_e = 1 cm) is about 4.5 db higher than that for the x-band (λ_e = 3.248 cm). The PSD at K = 70-80 is lower than that at k $\sim$ 20-30. However, backscattered power is proportional to k^3 x PSD (two-dimensional case). All this means is that with the capillary waves present, the PSD is decreasing more slowly than k^{-3}.

Scattering from the background wave form can be analyzed in the same spirit. Suppose we choose to think of the unperturbed profile as a sharp wedge. The background wave form can be obtained from the sharp wedge through the following series of deformations: (i) rounding the tip of the wedge, (ii) making the front face concave, and (iii) making the back face concave. This is shown in Figure 20. It is not difficult to see that rounding the tip off the sharp wedge is a small perturbation. There is a slight complication, however. The difference in scattering amplitude between the sharp wedge and the rounded wedge is slightly smaller (about 2 db) than the scattering (either by numerical computation or SPT) due to the sharp tip being put on a horizontal plane. The reason is that the sharp tip has a maximum slope of $\sim$ 20°. When the incidence angle is 67.7°, in addition to direct scattering from the tip, there is double reflection between the flat plane and the tip. In a sense, the tip and the horizontal plane act like a corner reflector, which is not the case when the tip is sitting on the rounded wedge. In any event, for smaller incidence angles and for larger wedge inclusive angles, the above effect is not present. In the case that we have considered, the roundedness decreases the scattering amplitude by about half, or 6-7 db. The concavity on the front face can also be considered in the same manner. It increases the scattering

in the case considered by about 2 db. The concavity of the back face produces hardly any change in the scattering. From the SPT point of view, this is quite obvious since the perturbation is on a slope of almost -20°, making the effective incidence angle almost grazing. The above exercise of decomposing the original wave into its various components serves the following purposes: (i) The relative importance of the different surface features is now understood. The "background wave form" is the predominant source of backscatter, typically accounting for 3 to 4 db more backscattering than the parasitic capillaries. The two contributions may be in or out of phase. (ii) The approximate scattering theories applicable for these different surface features are also established. The parasitic capillaries scatter in a small perturbation manner, whereas the background wave form scatters as a (a) sharp wedge (GTD) - (b) rounded tip (SPT) + (c) concave front face (SPT). The range of usefulness of an approximate theory depends on the extent in which the required conditions are obeyed. We have seen that understanding the parasitic capillary scattering in terms of SPT is highly accurate whereas thinking of "background wave form" scattering as GTD wedge diffraction requires considerable correction. Even with the rounded tip and concave front face added, the agreement can still be 1-2 db off. The quantitative usefulness of an approximate theory in this case is therefore limited. Rather the decomposition of the background wave form into its subcomponents provides us with insight into the nature of the scattering. It also enables us to understand why the background wave form cannot be described by SPT. (iii) The frequency dependence of scattering may now be predicted. At Ka band, for example, we can expect the scattering to be coming more from the parasitic capillaries, which may now be truly "resonant", and less from the "background wave form", which may be too rounded to have any

resemblence to a wedge. At frequencies lower than x-band, exactly the opposite may happen. In retrospect, x-band may happen to be the awkward frequency at which the small radius crest and the parasitic capillaries have competing significance.

We have thus far analyzed the nonspecular events, which besides being susceptible to numerical analysis, are also more frequent. The specular events have been investigated with flash photography. Figures 21(a) and 21(b) are examples of this. Figure 21(a) shows a case where the specular facets are point-like, which is representative of specular reflection from a highly turbulent wake. Figure 21(b) shows a case where the specular facets are line-like and ring-like, which is representative of specular reflection from a steep capillary wave. It can be seen that for these specular events, vv and hh scattering amplitudes are very close, sometimes almost identical, especially for smaller incidence angles like 40°. The percentage of specular events among all scattering events is probably a very sensitive function of the amplitude, steepness and surface clearliness of the waves. Our rough estimate shows that at 40°, about one third of all events are specular. At 70°, about one sixth of the events are specular. But even up to 70° incidence angle, specular events play a significant part in the overall scattering process, since they are usually the events with the largest amplitudes. The significant contribution of specular events, which the composite model has completely neglected, is probably the major reason that the polarization ratio in a rough ocean is smaller (i.e., closer to 0 db) than would be expected.

We have also attempted to study the Doppler shifts of the specular events using double flash photography. Between the flashes (which are 20 msec apart), the specular points can be seen to have moved forward in the photographs. Some

representative points per event can be chosen and their velocities measured and compared with the Doppler shift. However, when this is done the variability of the velocity of the specular points is found to be too great so that the comparison is not very meaningful.

We have not attempted to study the absolute backscattering amplitude of specular events in terms of the photographic brightness of the specular points. Although conceptually this seems a worthwhile thing to do, we do not think that our present set up will yield very quantitative results. The importance of specular reflection warrants a separate study by itself.

VI. CONCLUSIONS

We have studied x-band microwave backscattering at moderate incidence angles from a mechanically generated wave train of short gravity waves (2.5 Hz, 25 cm). We have found that for water wave trains with small amplitude, there is hardly any measurable microwave backscattering. As wave amplitude is increased, however, beyond a certain threshold, backscattering quickly appears. This threshold corresponds to the onset of self modulation in the wave train. At a steepness of ka = 0.17, the self modulation is such that at 8.4 m fetch, one out of every three or four waves attains a small enough radius of curvature at the crest that it undergoes breaking with capillary waves being radiated down the front face. A turbulent wake may or may not appear behind the crest. We refer to this kind of breaking as "gentle breaking" since it does not involve bubbles or spray. For wave trains under these conditions, we observe that the backscattering occurs as discrete bursts (rather than as a white-noise-like continuous return) and the bursts strongly correlate with the "gentle breaking" events. The discreteness of the bursts implies that the scattering sources are localized on the surface. These discrete scattering events have been carefully studied and can be separated into two categories: (a) non-specular events, and (b) specular events, which may have a small hidden non-specular component.

The specular events have been studied with the aid of flash photography. We have found that the frequency of specular events varies from roughly one third of all events at 40° incidence to roughly one sixth of all events at 67.7° incidence angle. The power of a typical specular event is usually two or more times higher than that of a typical nonspecular event. The polarization ratios of specular events at 40° and 55° incidence angle are very close to

0 db. At 67.7°, the ratio is slightly higher. The occurrence of specular events like these may be the primary reason for the ocean polarization ratios being closer to 0 db than expected. The Doppler shift of specular events indicates a surface velocity close to the phase velocity of the short gravity waves, i.e., $\sim$ 62.5 cm/sec. Our flash photographs show that specular reflection comes either from a very turbulent wake, in which case bright dots appear in the picture, or from steep capillaries, in which case lines or rings appear in the flash picture. Although our brief study here does not do justice to the importance of specular reflection, it does serve to point out that the potential significance of specular backscattering from the ocean at moderate incidence angles ought to be investigated.

The nonspecular events have been investigated using the deterministic approach. We have demonstrated the feasibility of the deterministic approach by comparing the measured results with numerically computed results in terms of absolute backscattered power, polarization ratio and Doppler shift. Having thus validated the approach, we have used it to show that the background wave form is the dominant scattering source, and that it scatters in a manner not describable by the small perturbation theory (SPT). A better description may be that of a wedge (describable by the Geometric Theory of Diffraction, or GTD) with a rounded tip (describable by SPT, which reduces scattering by about 6 db) and a concave front face (describable by SPT, which increases scattering by about 2 db). We have established that the wedge-like character of the crest is the reason that the background wave form is not describable by SPT. It is also probably the second reason why the ocean polarization ratio is smaller than expected. The Doppler shift associated with the background wave form corresponds to the phase speed of the short gravity waves, i.e., 62.5 cm/sec. The parasitic capillaries also scatter, but their contribution is usually a

few db smaller than that of the background wave form and it may be in or out of phase with the background wave form. The polarization ratios measured at all incidence angles are smaller than those obtained if scattering came solely from capillaries on inclined planes scattering in the SPT manner, which is consistent with our results for the scattering contribution of the background wave form. The Doppler shift associated with the capillaries corresponds to speeds within ± 10% of the gravity wave phase speeds, an indication of the parasitic nature of such capillary waves. The parasitic capillary scattering can be completely understood in terms of SPT although the dominant wavelength of the capillaries is far from being "resonant" with x-band at moderate incidence angles. We can say that it is the capillary induced surface roughness which is scattering in a small perturbation manner. One implication is that Ka-band or higher microwave frequencies may be better frequencies for sensing these parasitic capillaries. Another implication is that for frequencies lower than x-band, say L-band, the scattering will become more wedge-like in character. (Of course, in the limit of even lower frequency, SPT will become applicable again at some point.)

In view of the long and widespread acceptance of SPT as the correct theory of microwave scattering from the ocean, the following three objections may arise in regard to our work: (i) that our horn is too focused to see the Bragg resonance phenomenon, which results in our seeing little of the Bragg resonance scattering, (ii) that the short gravity waves we have investigated are artificially devoid of high frequency Bragg waves, which should be more prevalent on a natural wind-generated surface like the ocean, i.e., our investigation may be irrelevant to ocean scattering, and (iii) that the preponderance of existing evidence clearly shows such good agreement with SPT or the composite

model that our suggestions of possibly new scattering features or mechanisms seem unnecessary. In reply to objection (i), we have tried generating sinusoidal wavelets and varying the frequency slowly through the Bragg resonance. At 54° incidence angle, we observed the resonance at 11.3 Hz with a 3 db width of 0.9 Hz and a polarization ratio of 11.4 db. This is in excellent agreement with SPT predicted values of 11.6 Hz and 11.9 db (assuming water to be dielectric, rather than as perfectly conducting). Thus if Bragg resonant components are present on a slightly perturbed surface, our horn is not too focused and will detect them. Indeed, some numerical modeling verifies this easily. Objection (ii) is a legitimate concern. We must say, however, that we are in no way trying to imply that ocean scattering is like scattering from our idealized, well-controlled water wave system. Indeed, there may be a large number of wind-generated slightly-rough patches on the ocean which satisfy the small perturbation criterion. In that case, scattering from these patches will be Bragg resonant in nature. However, our experiment shows the ease with which sharp crests on water waves can be created. The attendant reflection from specular facets and wedge-like diffraction from rounded crests are completely absent from SPT or the composite model. The existence, or absence, of such strong scattering features on the ocean surface must be investigated before they can be prudently ruled out. For objection (iii), we must look at the existing evidence carefully. So far, there has been no experiment showing that absolute backscattered power is related to the ocean surface spectrum in the SPT prescribed manner. This experiment would be very difficult, if not impossible, to perform. The ocean polarization ratio is sufficiently small in a rough sea that unreasonably large long wave slopes would be required to account for it using the composite model. There has been only sketchy data

about the Doppler shift of backscattering from the ocean. Perhaps the most quoted proof of the correctness of SPT and the composite model is that when backscattering cross-sections at different incidence angles and frequencies are measured, applying SPT gives an inferred ocean spectrum of $\sim k^{-4}$, agreeing roughly with existing theory. However, as we have shown, an ocean made up of waves like sharp wedges would also have a k^{-4} spectrum (in the high frequency limit) and the frequency dependence of scattering would be similar. This is therefore not a conclusive proof of the correctness of SPT or the composite model. If evidence is reviewed in this critical light, the conclusion that either SPT or the composite model is well tested and proven seems premature.

Our study of mechanically generated wave trains is intended to be a first step in the study of progressively more complicated and more realistic wave systems. It is our hope that the knowledge gained at each step will help us decipher the scattering signatures in the next. A detailed study of scattering from wind waves in the laboratory will be presented in a later report.

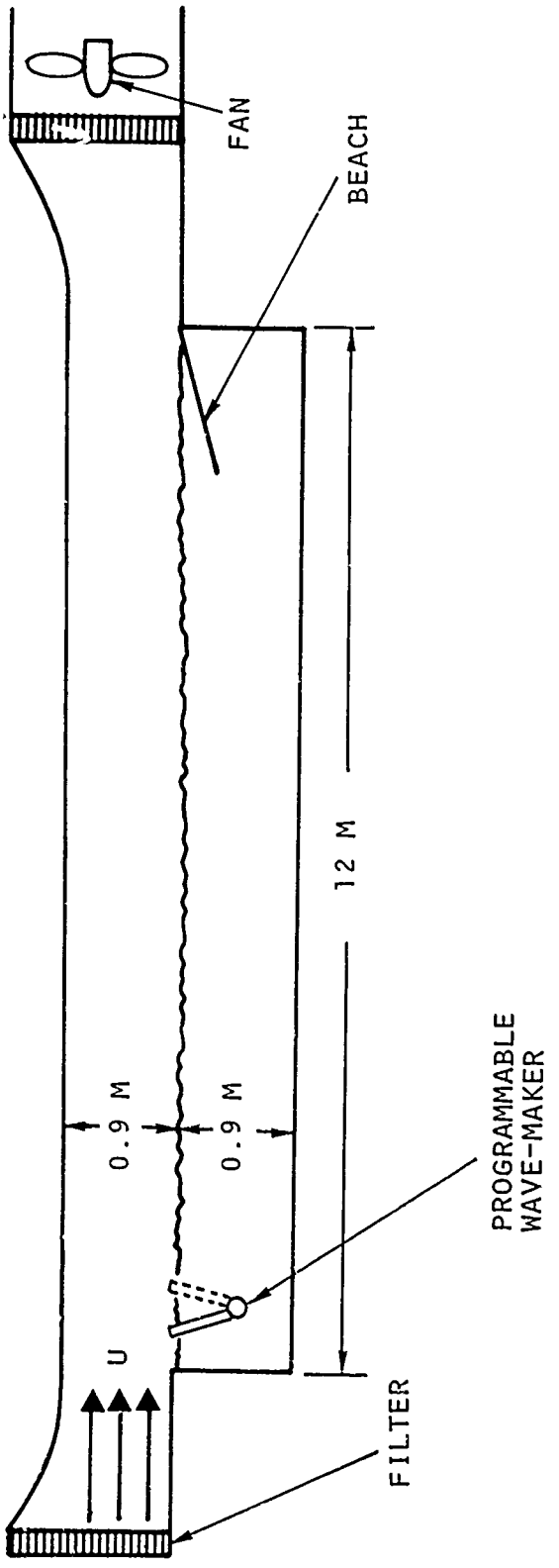

Fig. 1 Wave-tank arrangement.

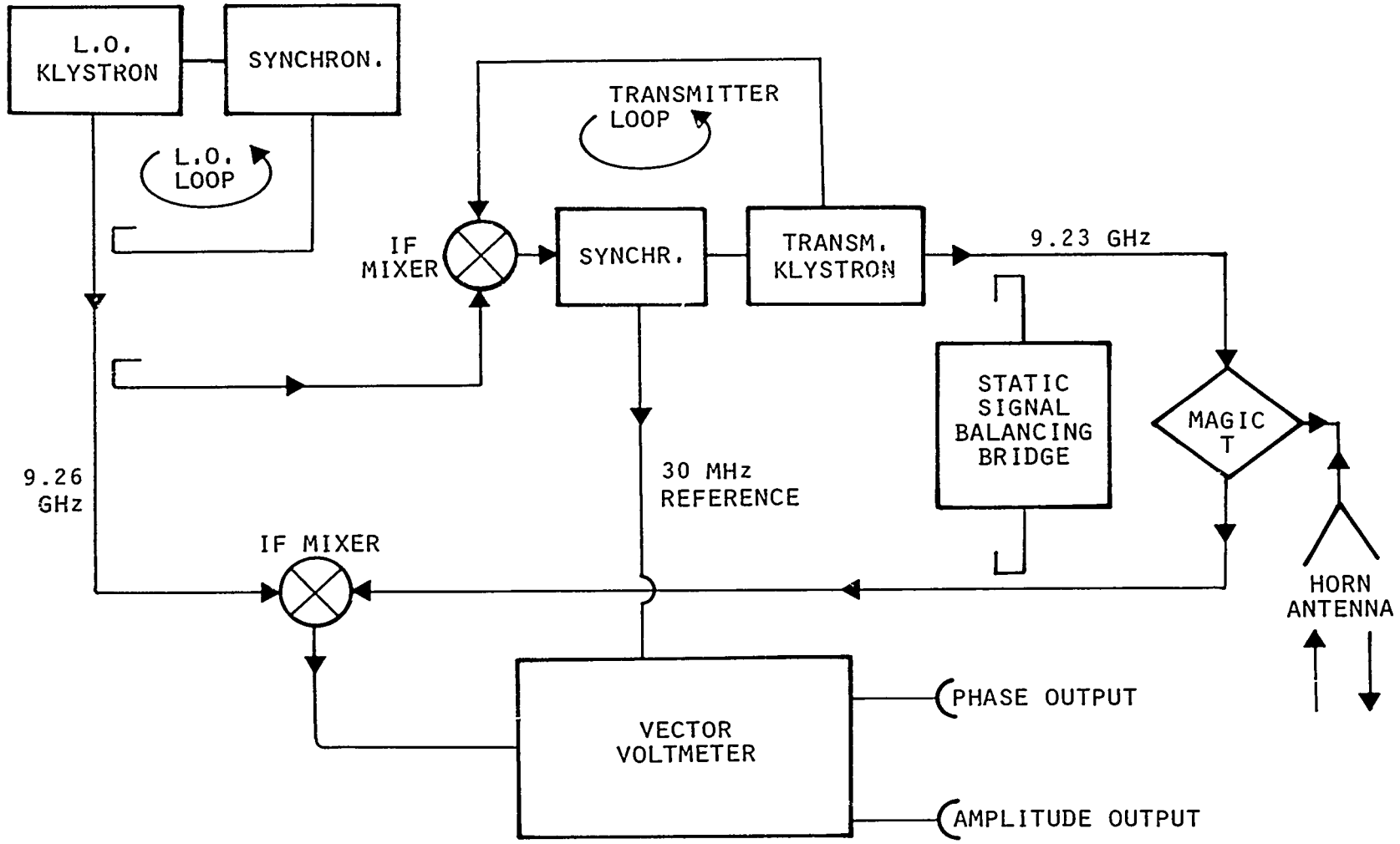

Fig. 2 Radar system schematics

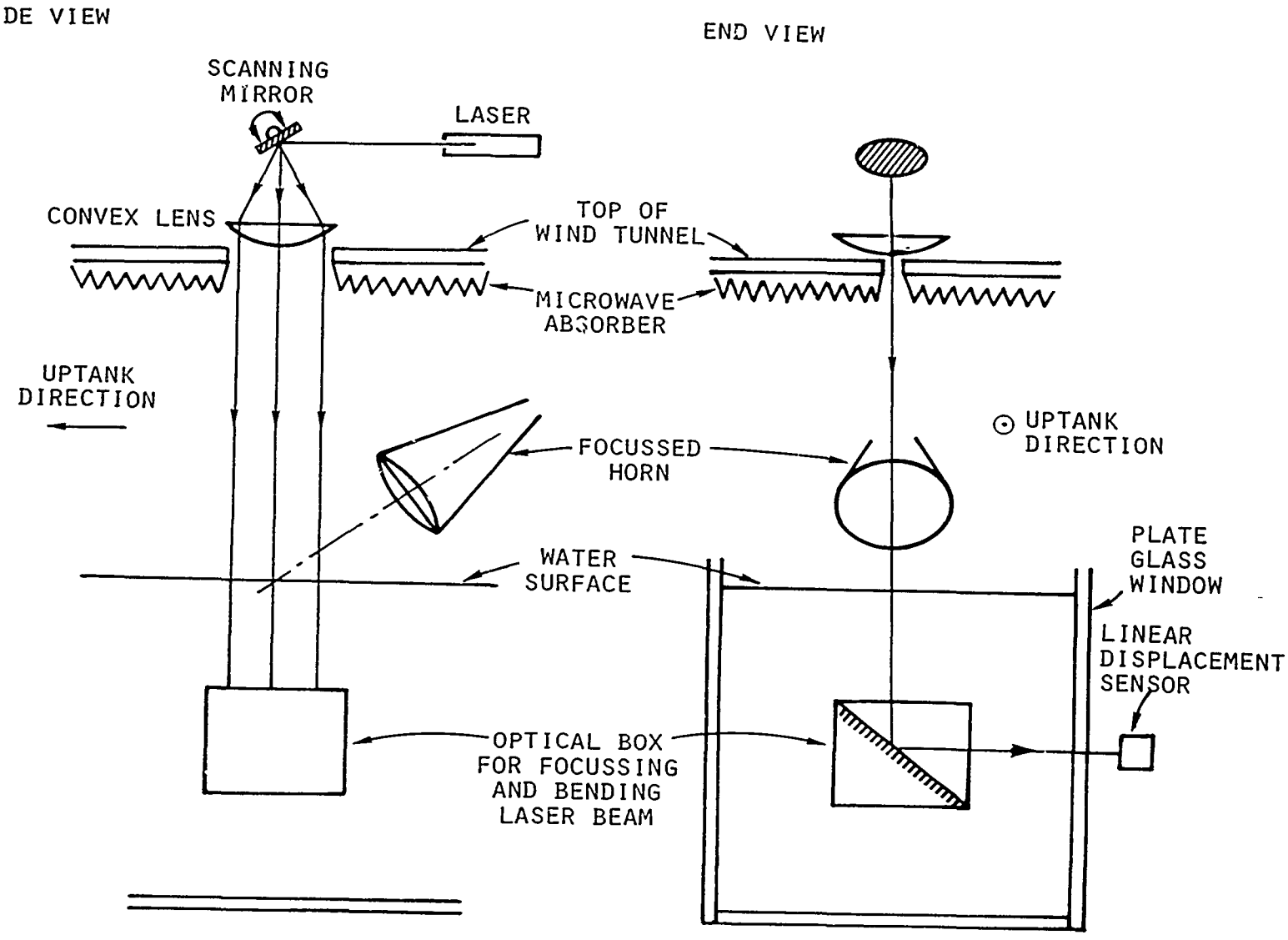

Fig. 3 Optical arrangement of scanning laser slope gauge

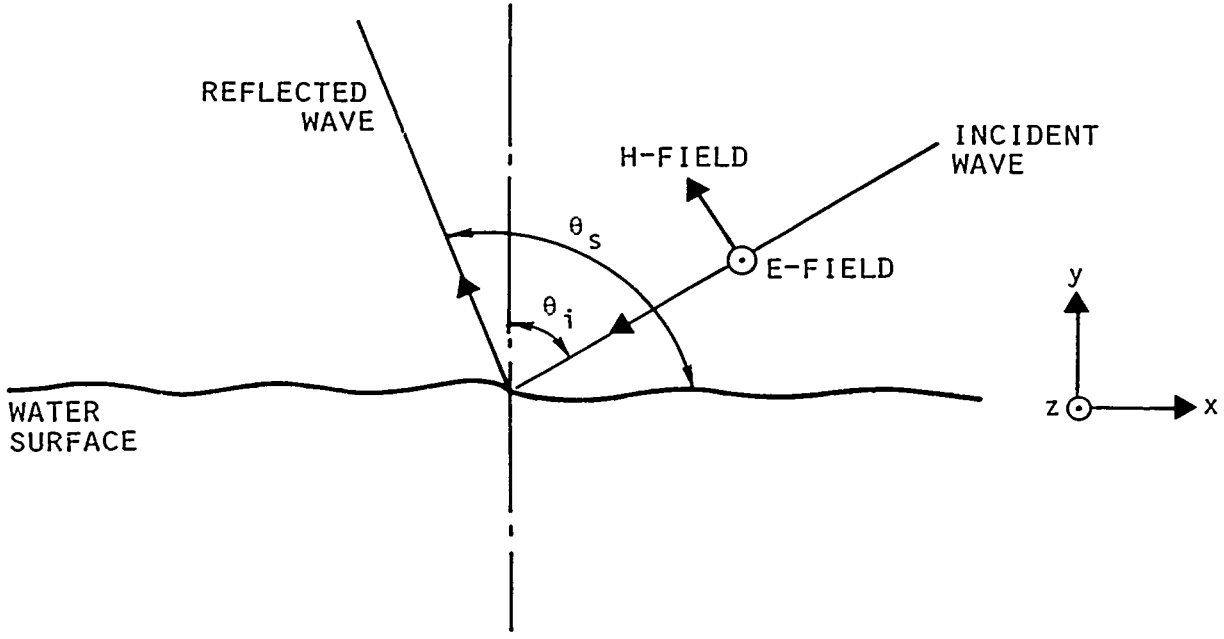

θ_i ≡ INCIDENCE ANGLE

θ_s ≡ SCATTERING ANGLE

Fig. 4 TM mode (hh polarization) field configuration

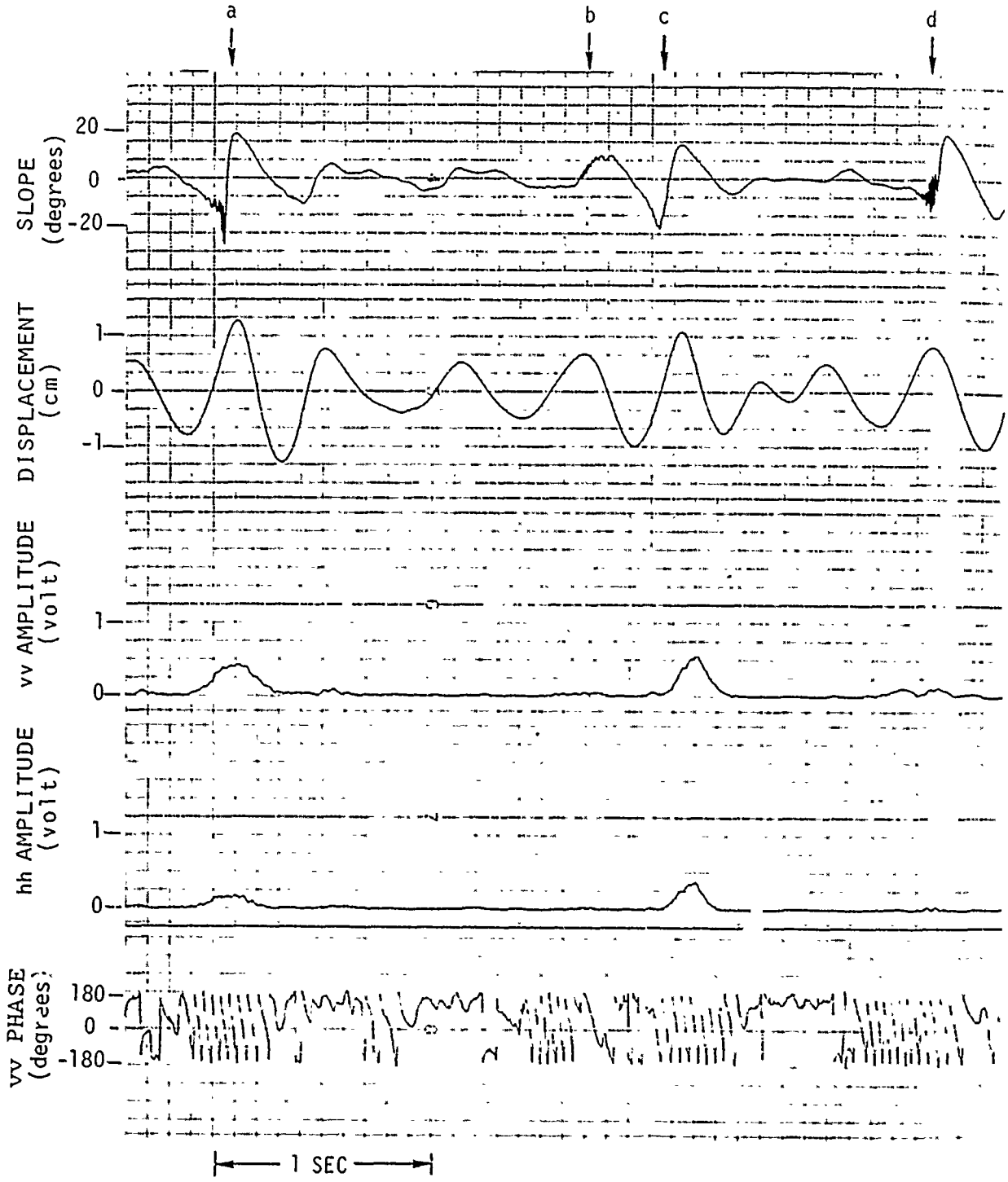

Fig. 5 Backscattering at 55° of microwave from 2.5 Hz modulated wavetrain. Slope is measured by stationary slope gauge. Displacement is measured by capacitance gauge at the same fetch but 45 cm to the side. vv and hh amplitudes are linear amplitudes, not power.

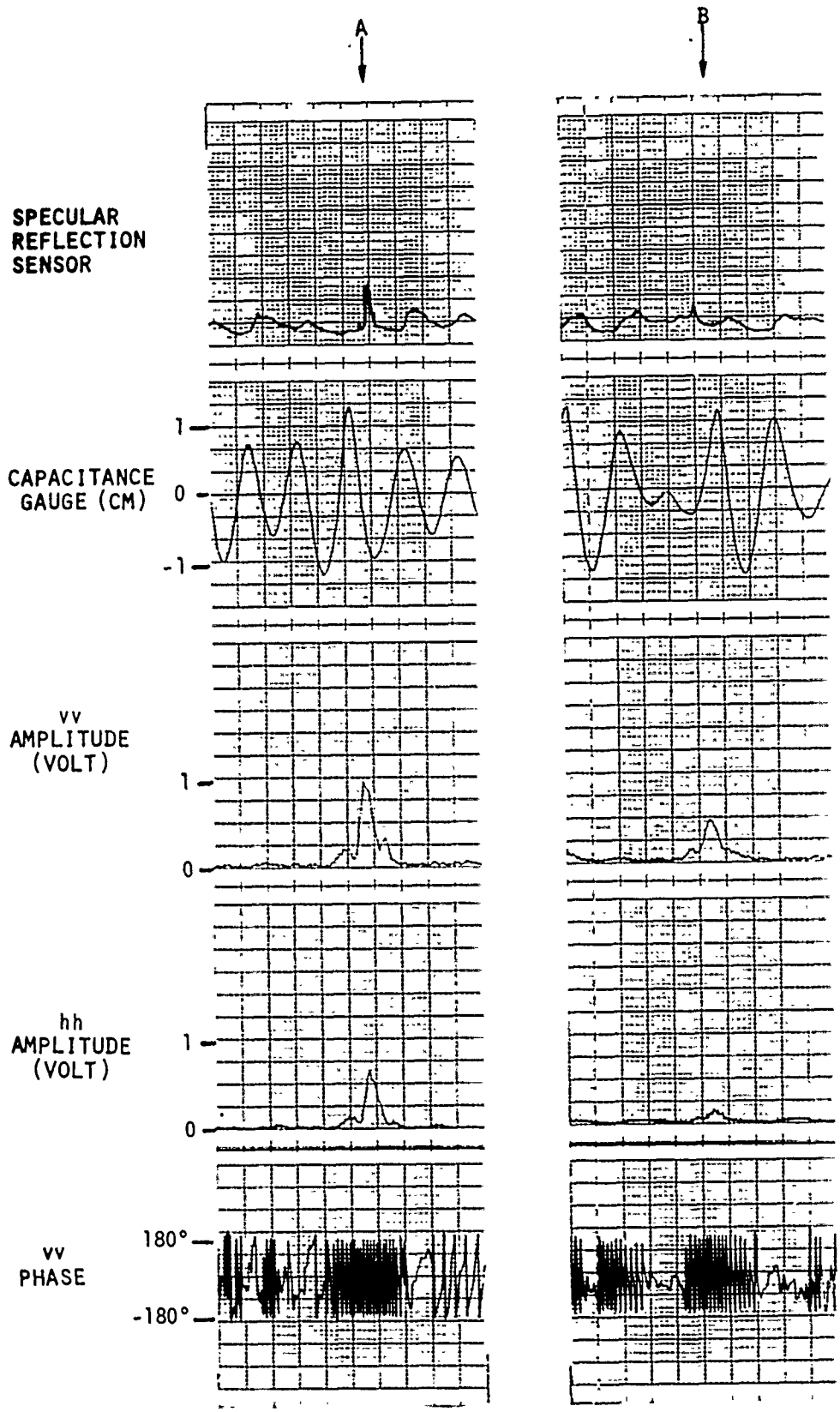

Fig. 6 Backscattering at 67.7° showing distinction between specular and nonspecular events. Event A is specular. Event B is nonspecular.

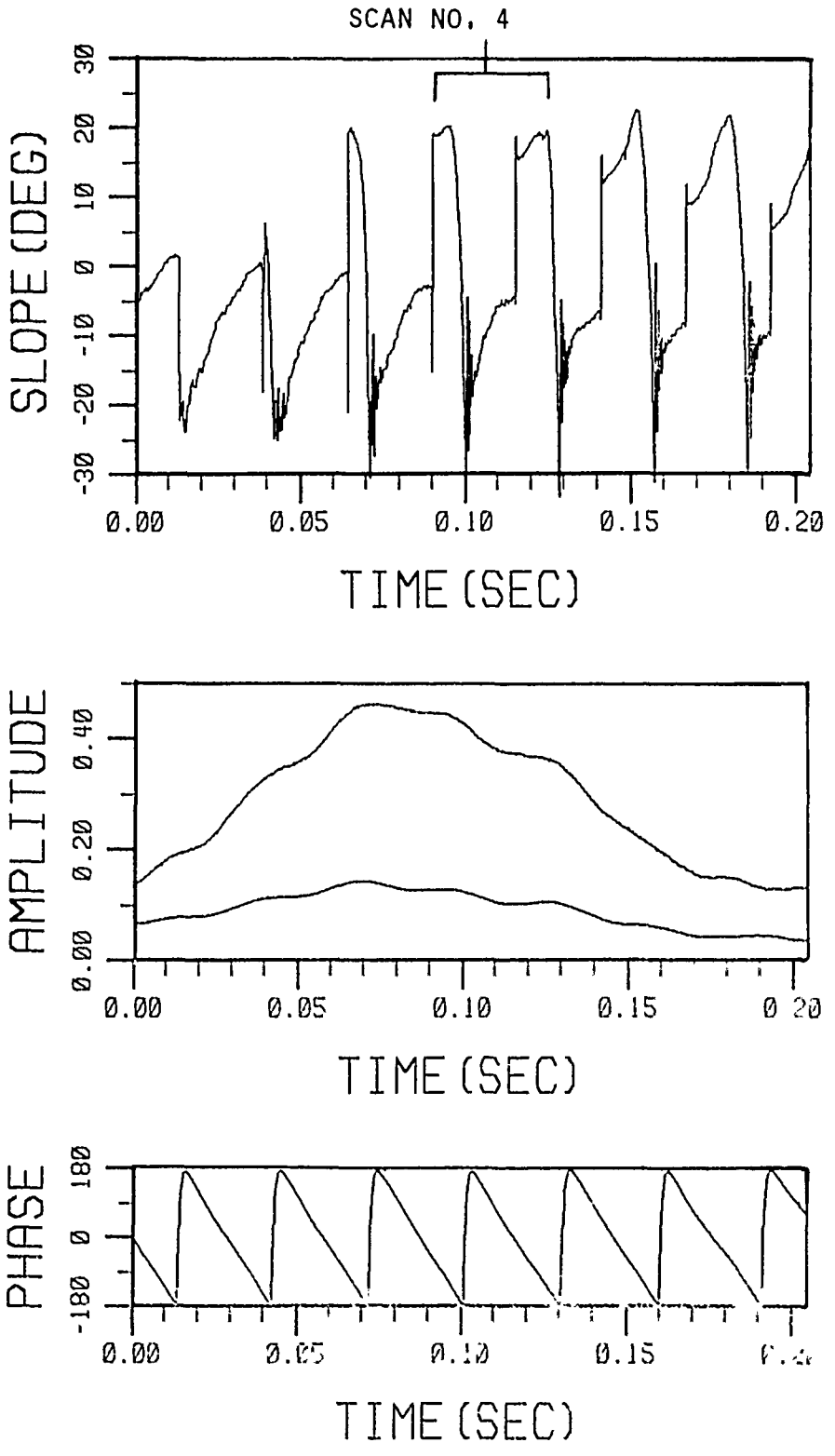

Fig. 7 Backscattering event B of Fig. 6 as recorded on the digital scope.

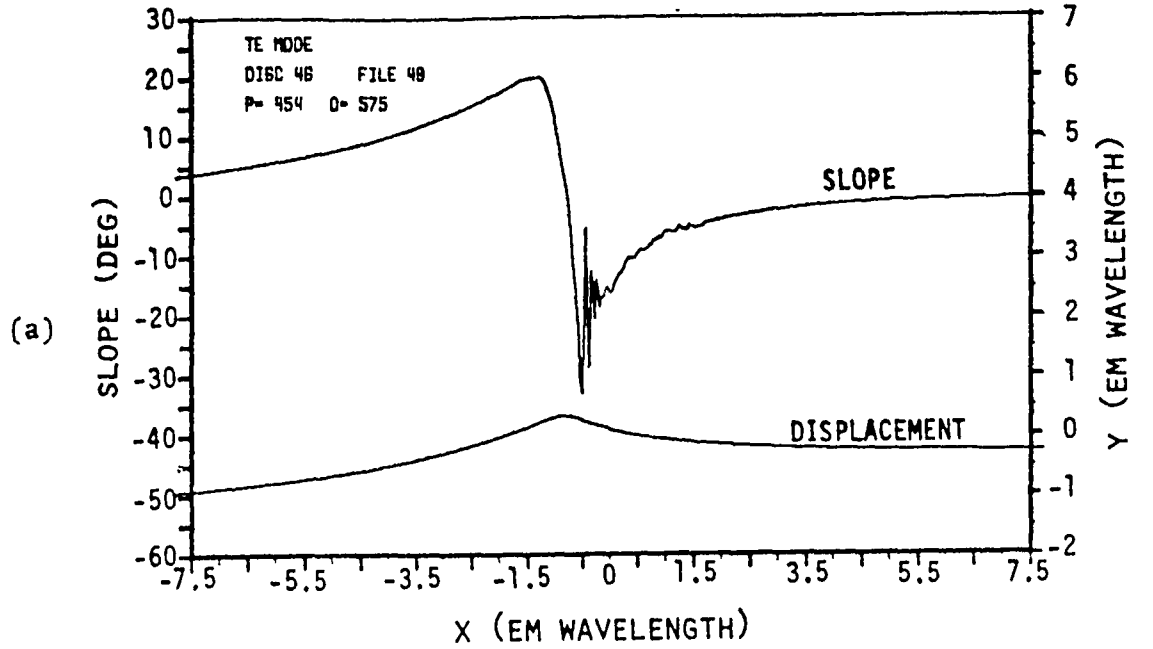

(a)

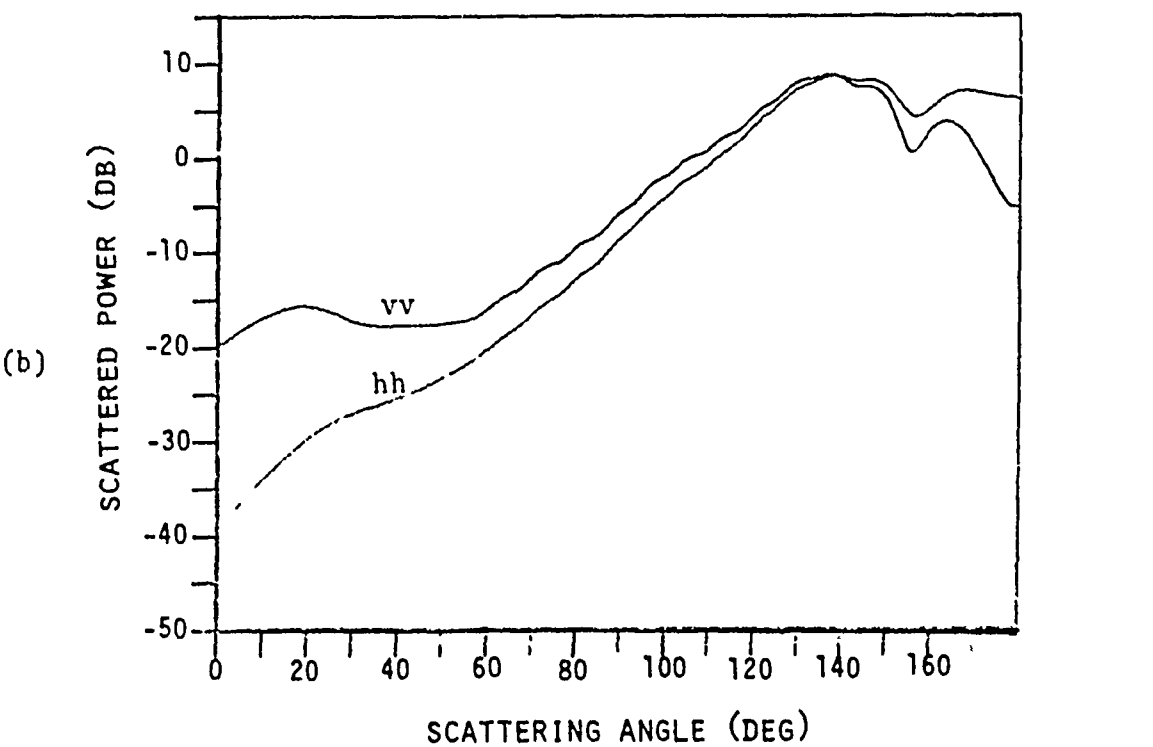

(b)

Fig. 8 (a) Slope and displacement profile of event in Scan No. 4 of Fig. 7
(b) vv and hh scattered power ($\equiv 20 \log_{10}|E_z^s|$) as a function of angle as computed by moments method.

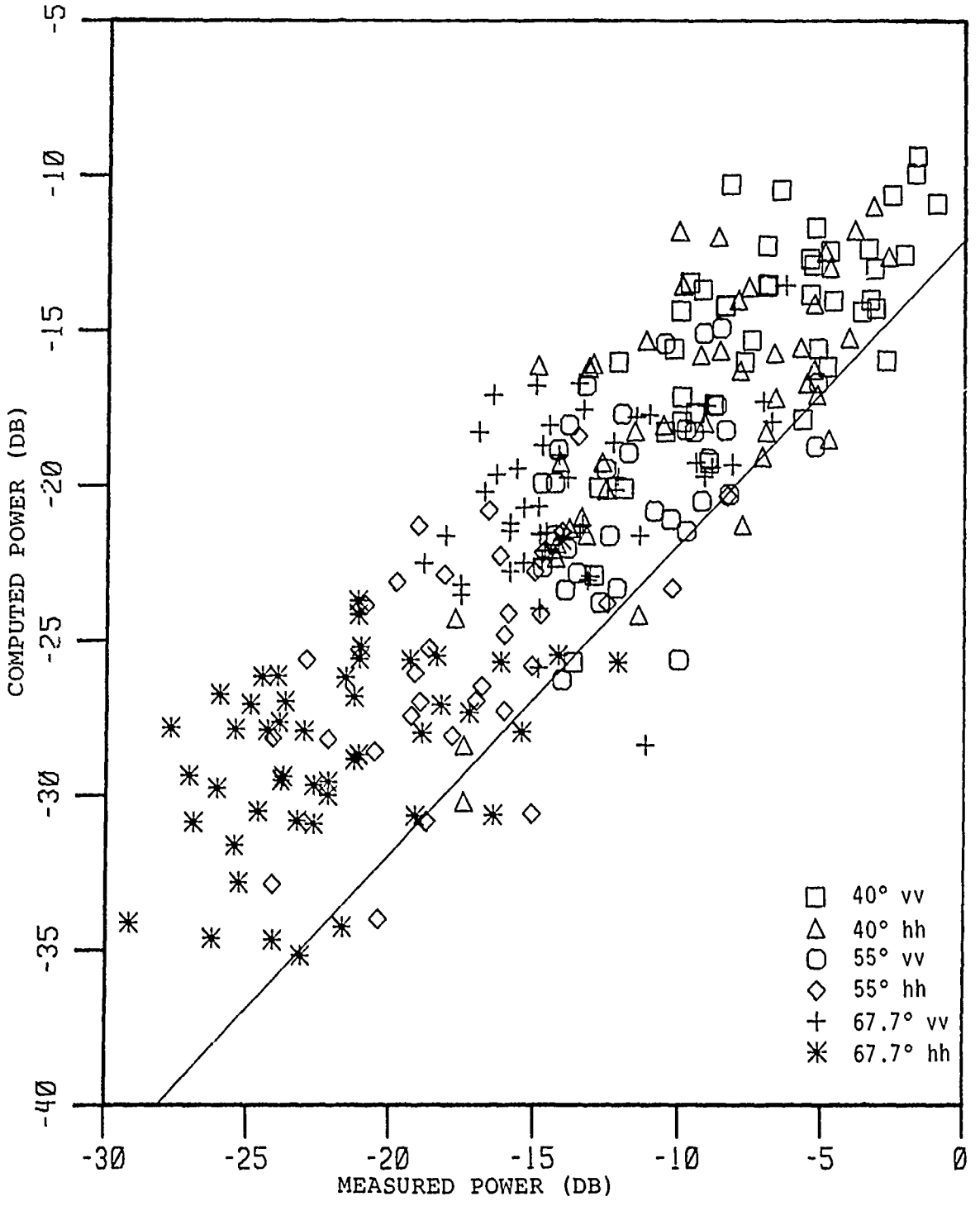

Fig. 9 Computed power (by moments method) vs. measured power in vv and hh polarizations for 40°, 55°, 67.7° incidence angles. Solid line is calibration line.

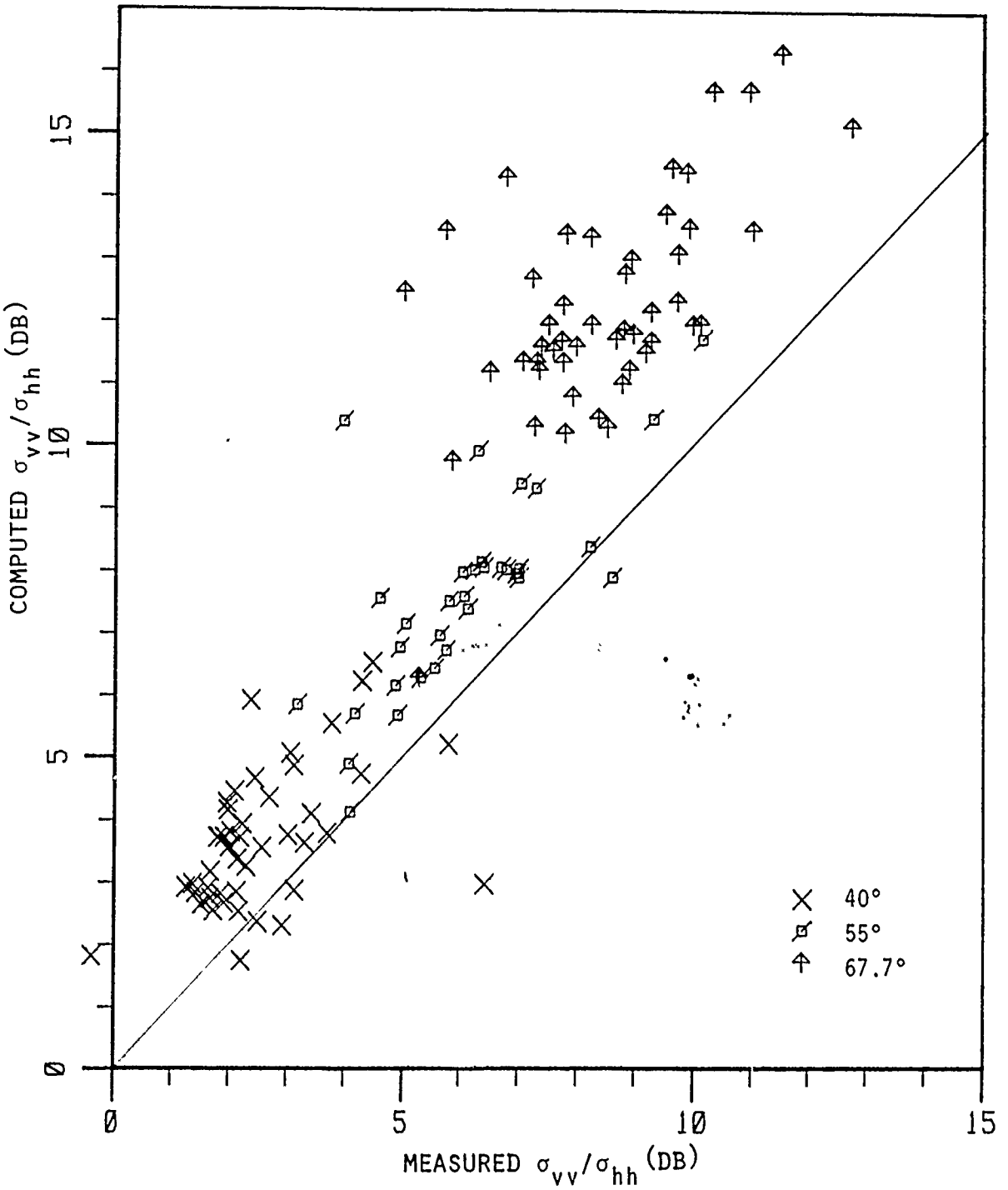

Fig. 10 Computed polarization ratio (by moments method) vs. measured polarization ratio for backscattering at 40°, 55°, 67.7°. Computation assumes water is perfect conductor. Solid line is 45° line.

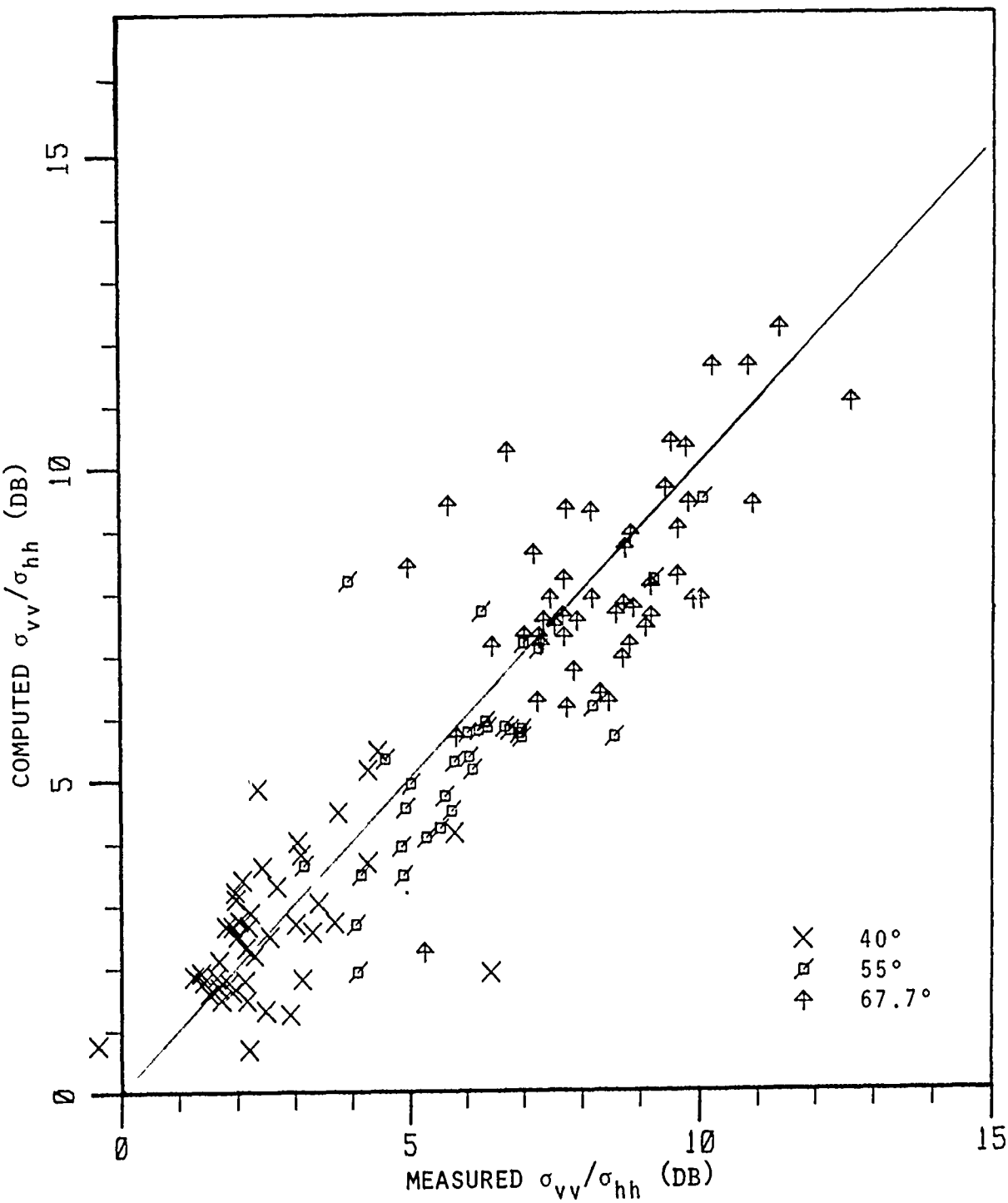

Fig. 11 Computed polarization ratio (by moments method plus small perturbation correction for water being a dielectric) vs. measured polarization ratio for backscattering at 40°, 55° and 67.7°. Solid line is 45° line.

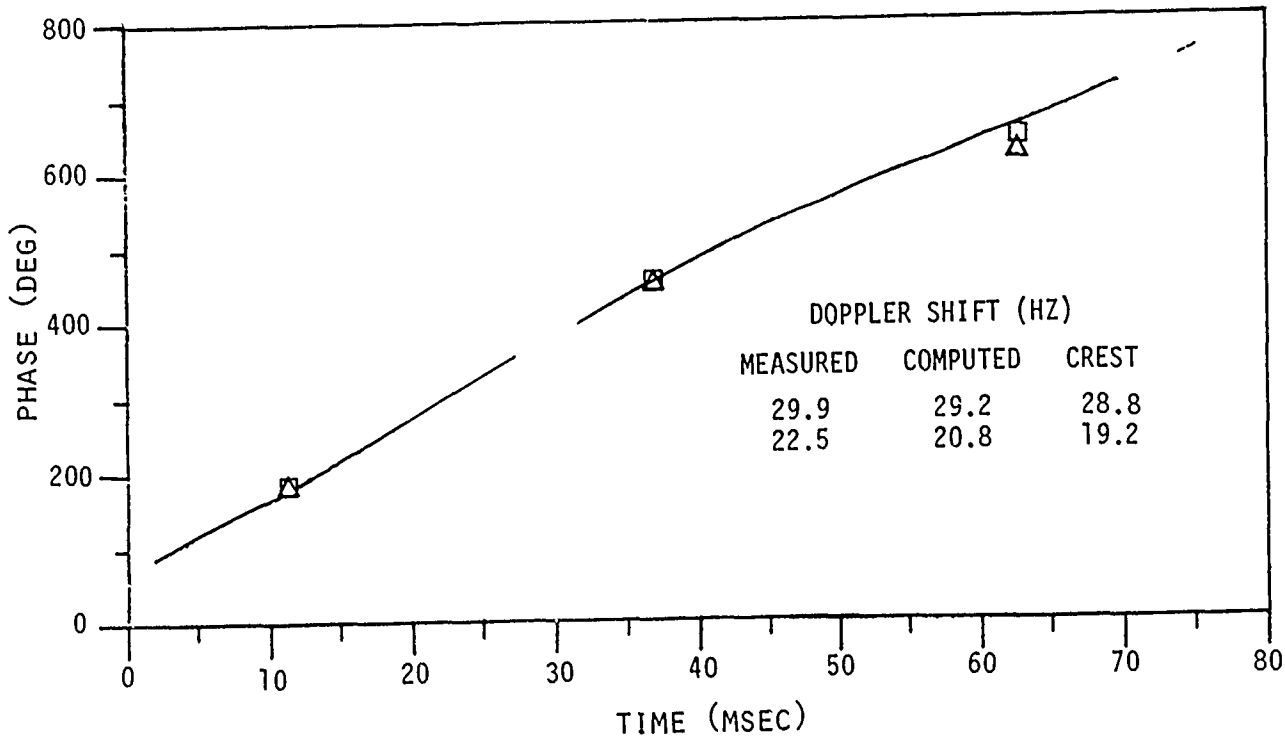

Fig. 12 Phase history of one event at 55°. Continuous line is measured phase of vv polarization. □ are the computed phases of 3 successive scans. △ are the phases of the crest locations in the same 3 successive scans. The Doppler shifts (△ phase/△ time) are also listed.

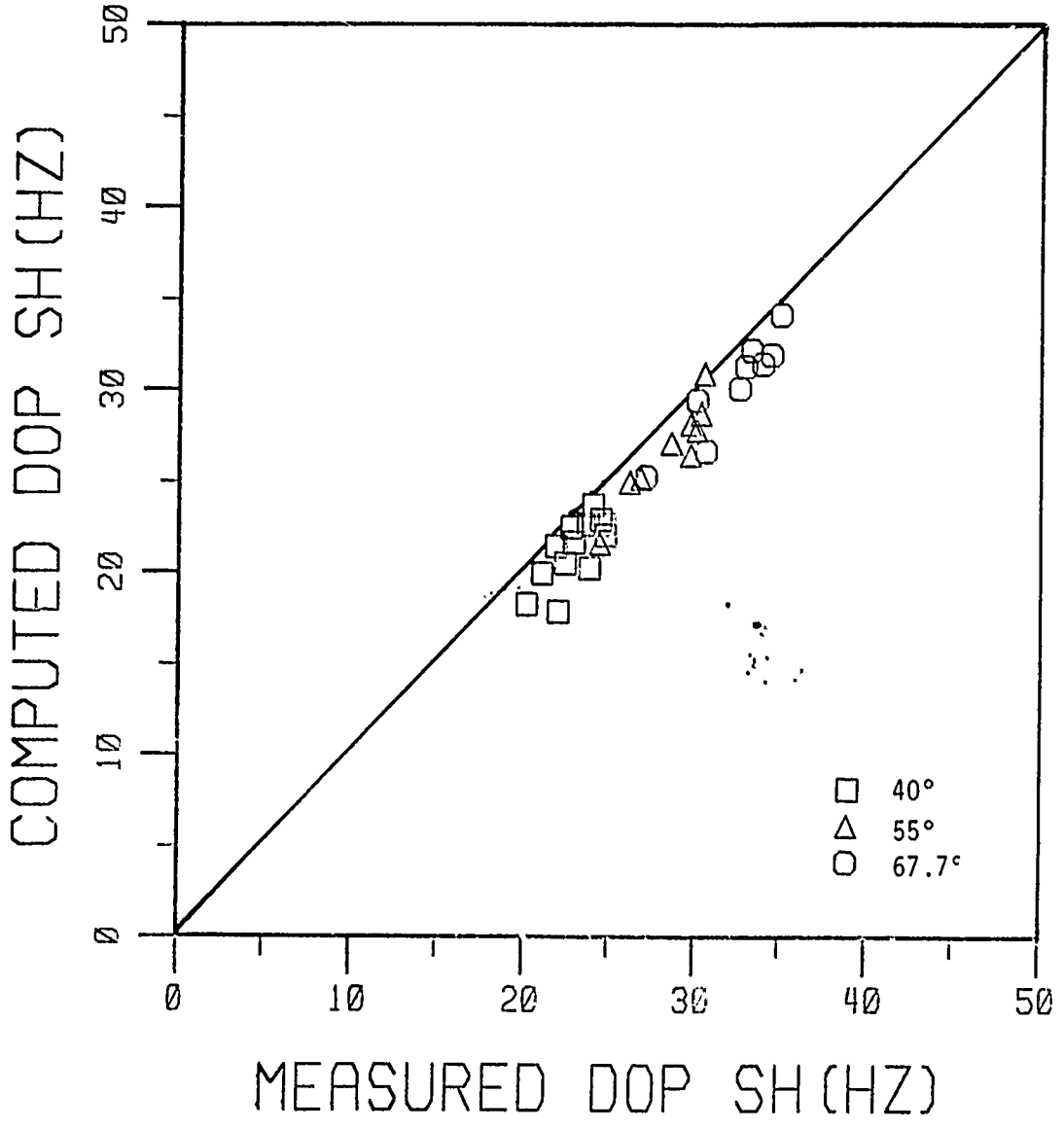

Fig. 13 Computed Doppler shift vs. measured Doppler shift for backscattering events at 40°, 55°, 67.7° from 2.5 Hz wavetrains. The solid line is the 45° line.

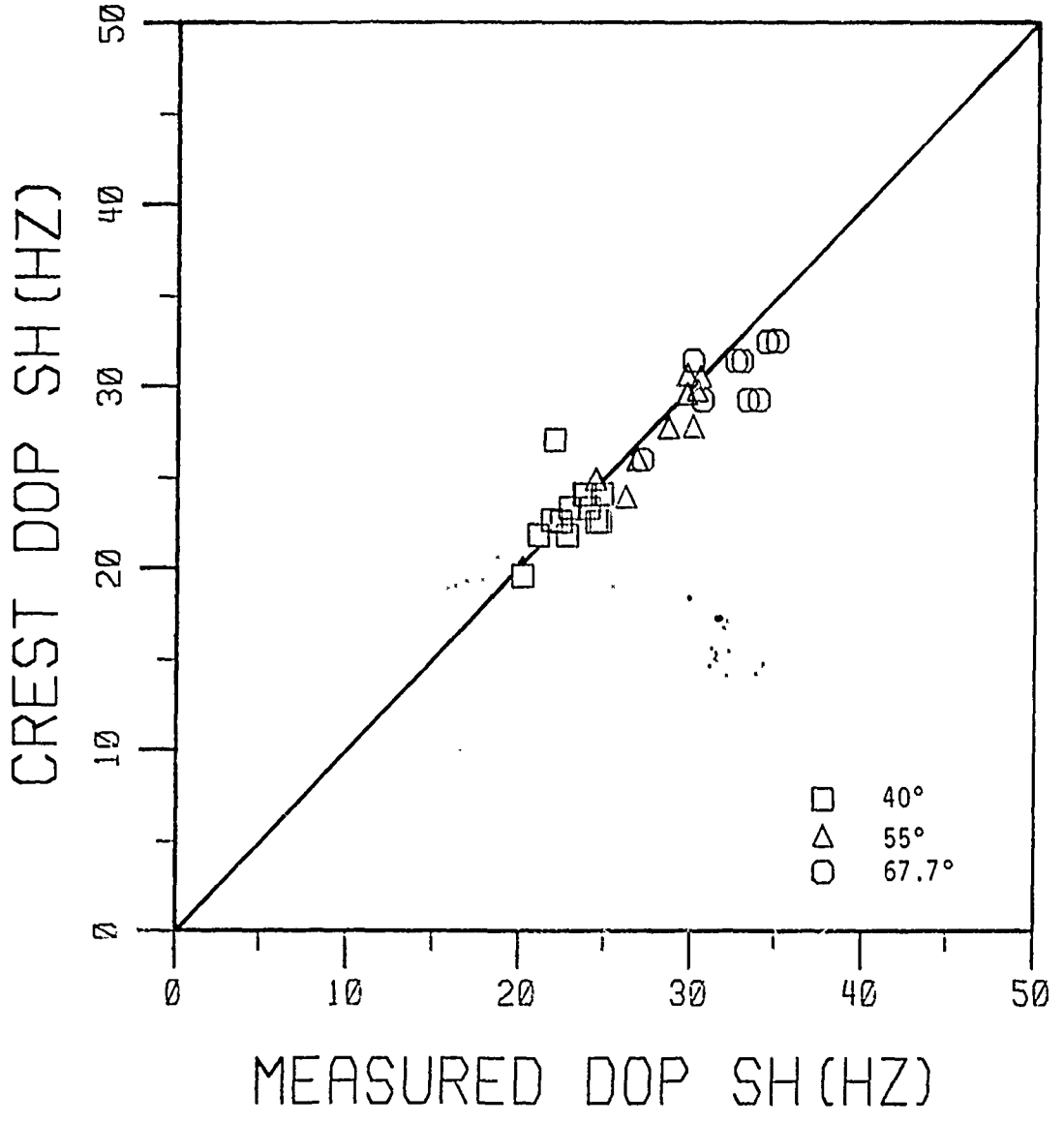

Fig. 14 Doppler shift of crest vs. measured Doppler shift for the same scattering events as shown in Fig. 13. The solid line is the 45° line.

(a)

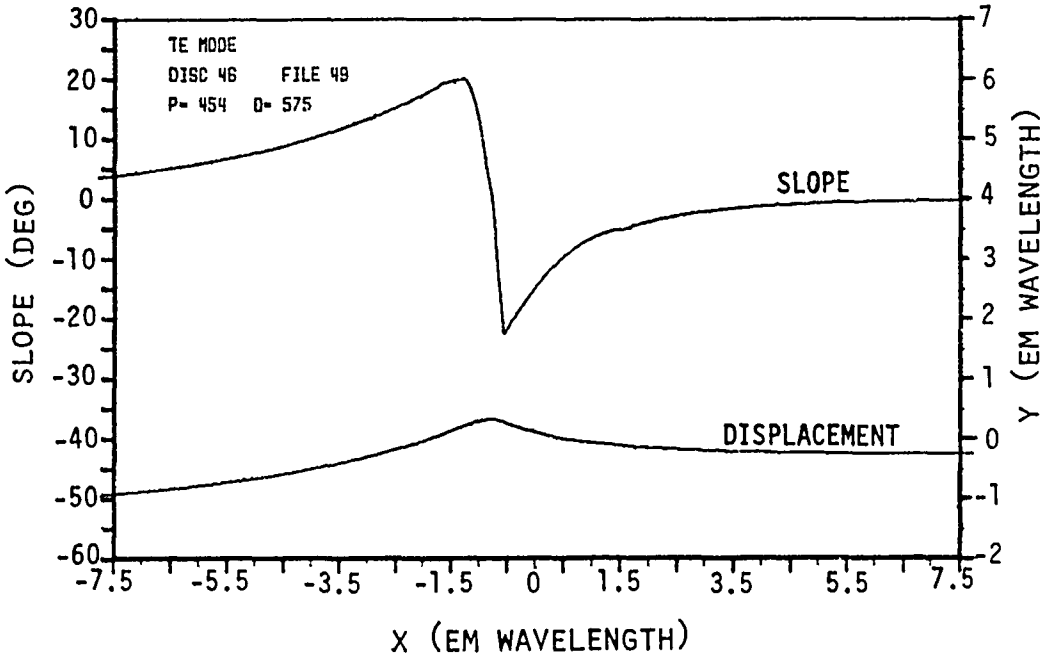

(b)

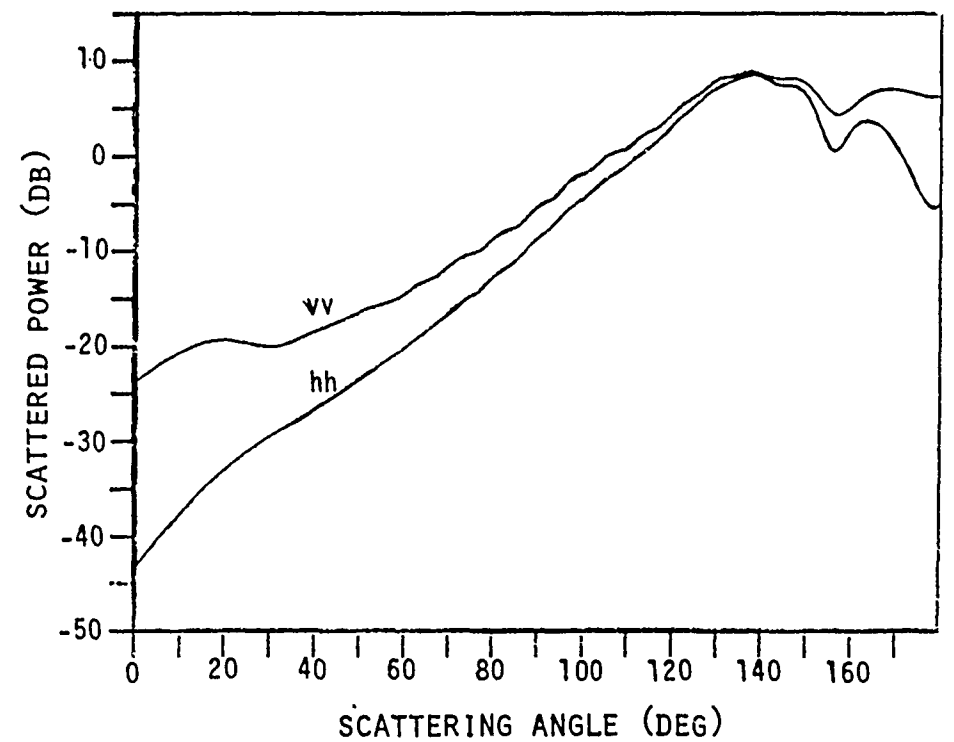

Fig. 15 (a) Wave in Fig. 8(a) with its capillaries smoothed away, leaving the "background wave form".
(b) Scattering from the "background wave form" as computed by the moments method for 67.7° incidence angle.

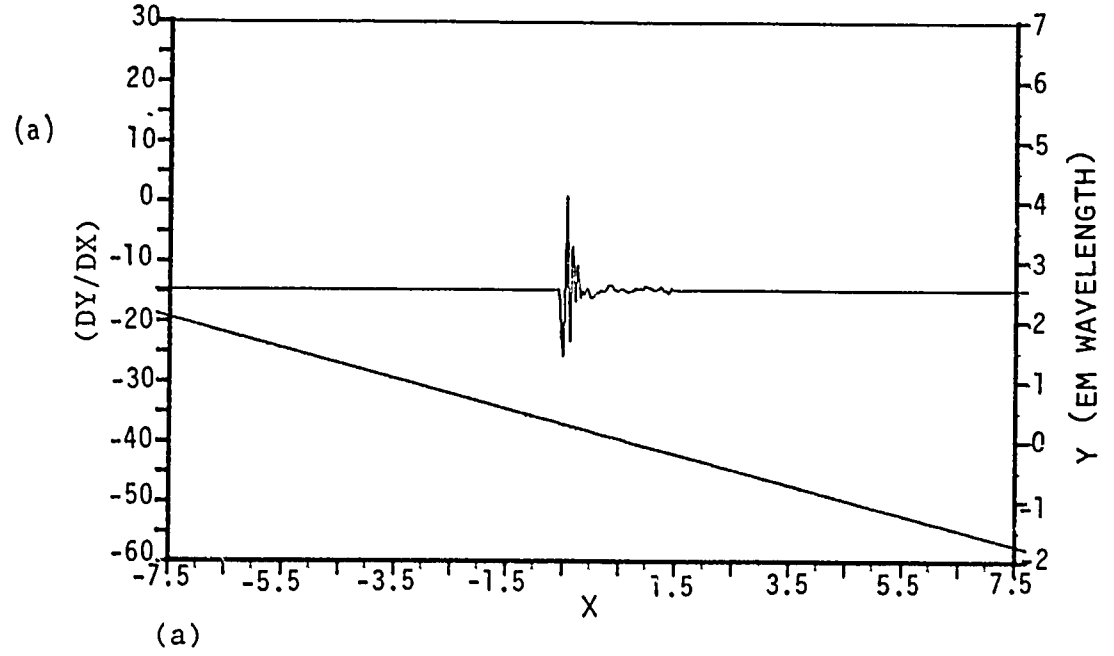

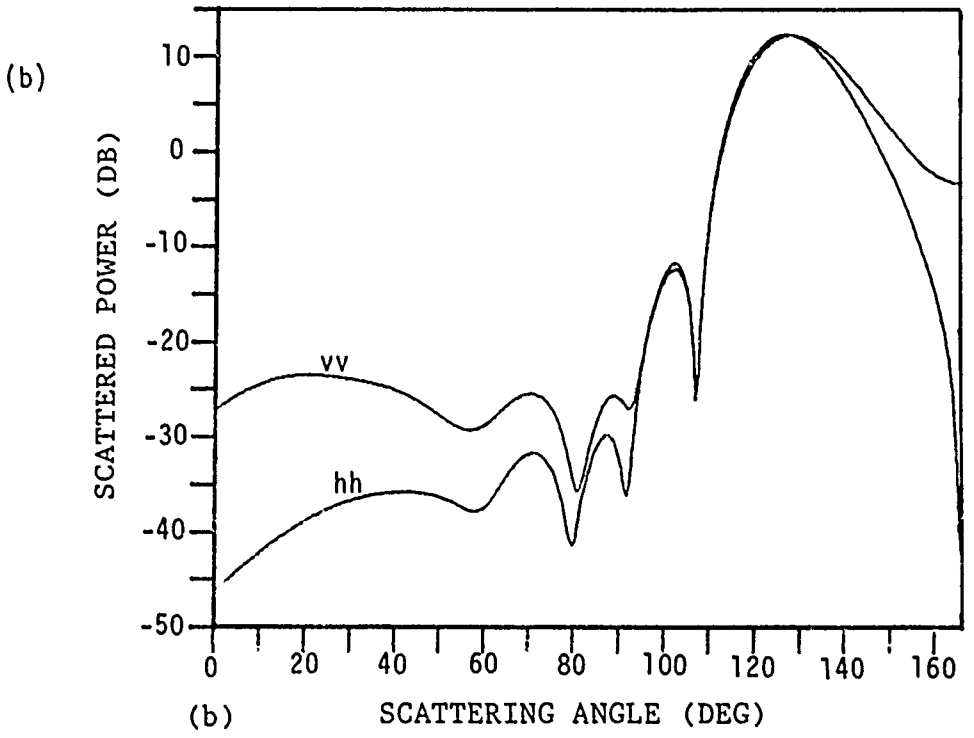

Fig. 16 (a) The parasitic capillary wave of Fig. 8 put on an inclined plane of 14.5°
(b) Scattering from the parasitic capillary on an inclined plane as computed by moments method for 67.7° incidence angle.

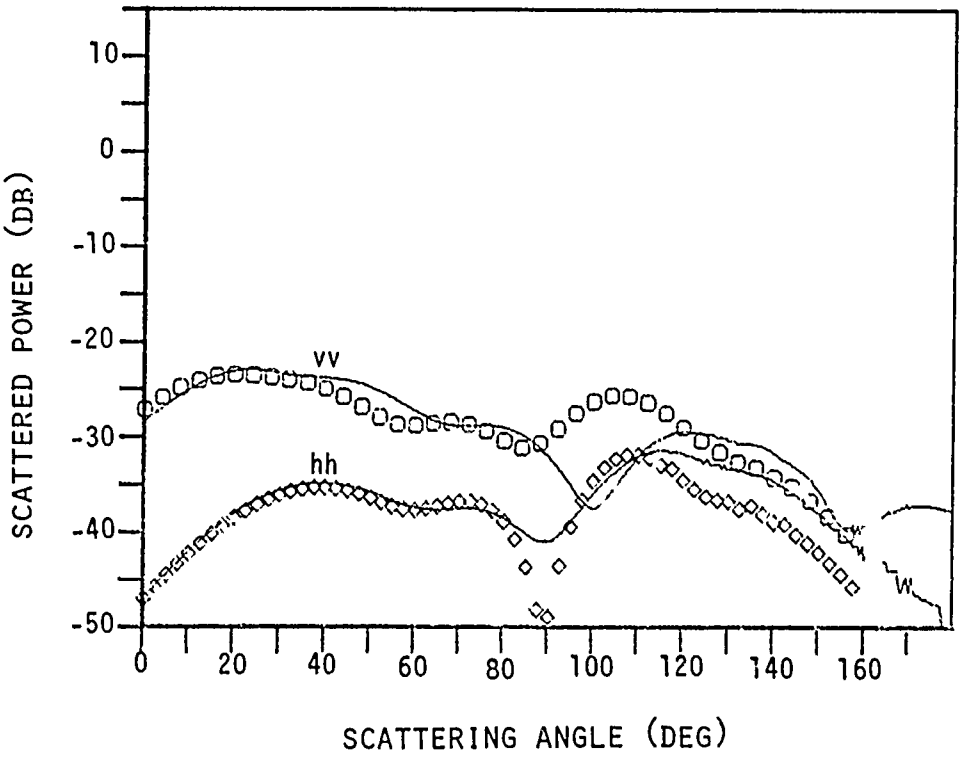

Fig. 17 Solid lines – difference between scattering from original wave (Fig. 8) and scattering from background waveform (Fig. 15). Symbols – difference between scattering from capillary wave on 14.5° inclined plane (Fig. 16) and scattering from flat 14.5° inclined plane.

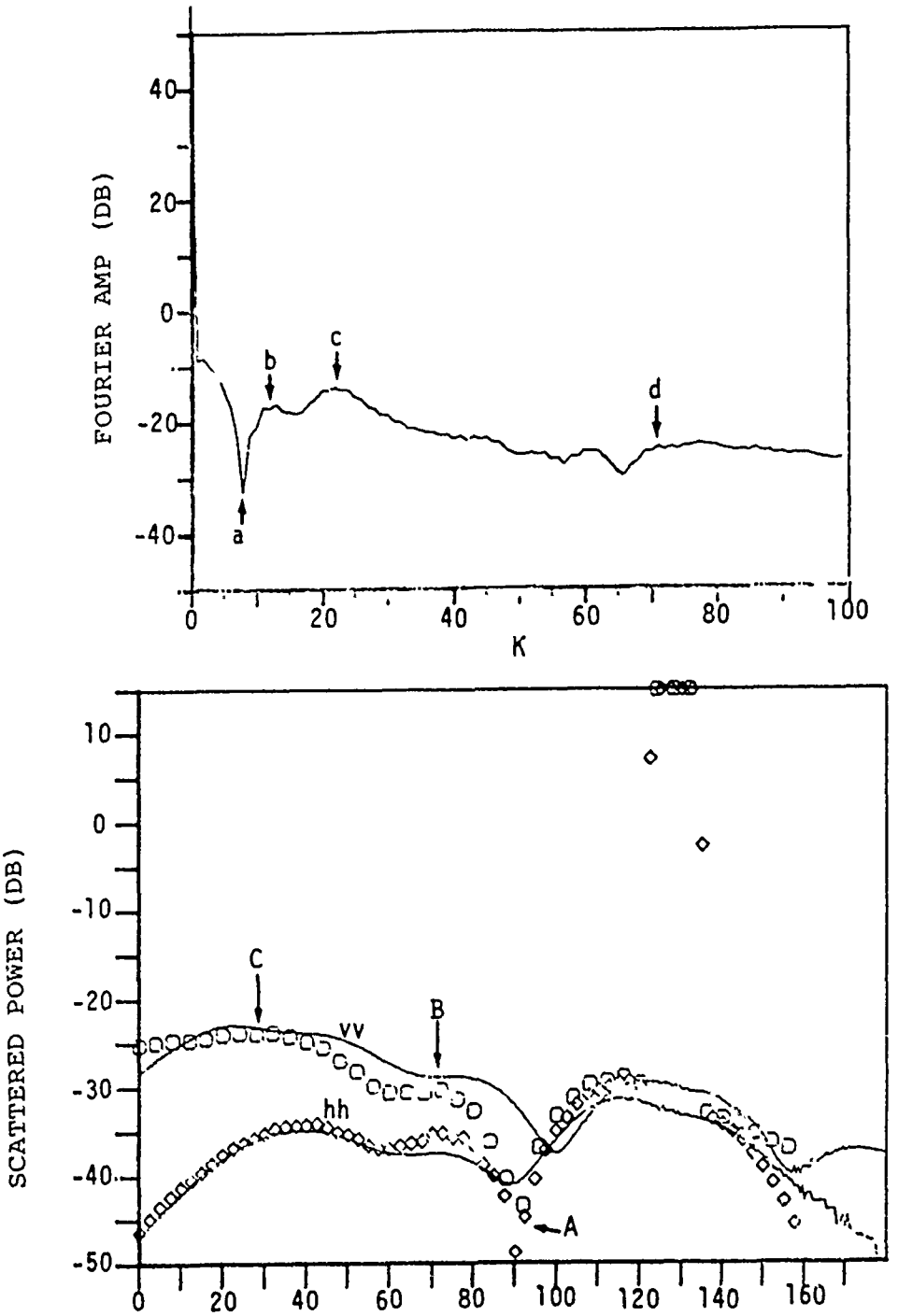

Fig. 18 (a) Fourier spectrum of capillary waves of Fig. 16(a) on a horizontal plane. Horizontal axis $K \equiv k \cdot L/2\pi$ where $k \equiv$ wavenumber, $L \equiv$ range in $x = 15\ \lambda_e$.
(b) Symbols — scattering as computed by SPT for 67.7° incidence angle. Capillary waves are assumed to be on a 14.5° inclined plane. Solid lines — difference in scattering from original wave (Fig. 8) and scattering from "background wave form" (Fig. 15).

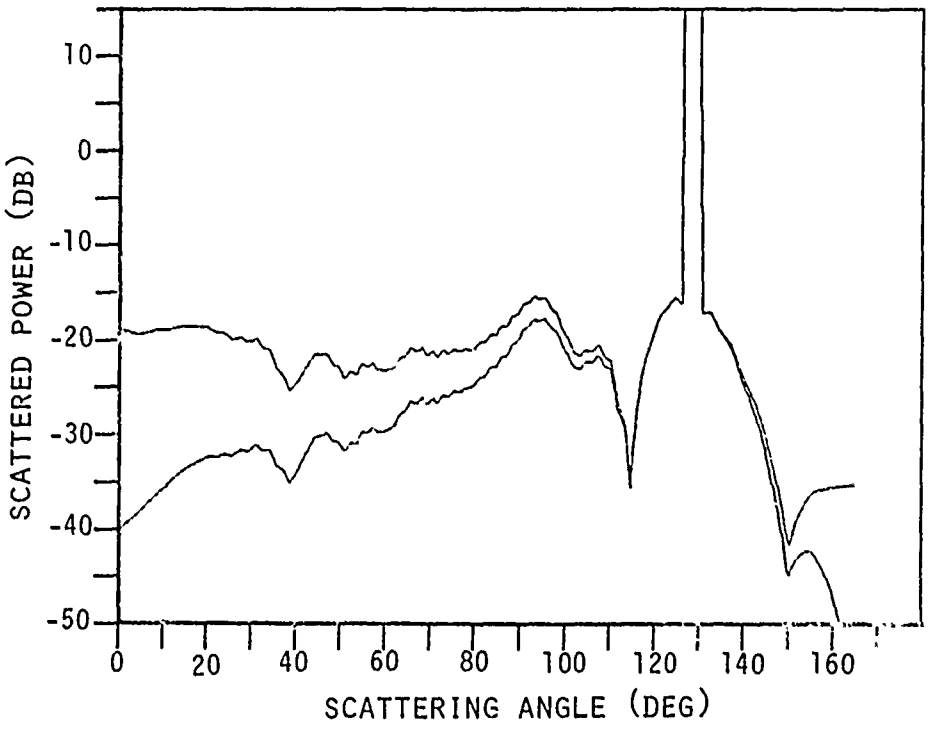

Fig. 19 Scattering from capillary wave of Fig. 16 as computed by SPT. λ_e = 1 cm (ka band), 67.7° incidence angle and inclined plane at 14.5°.

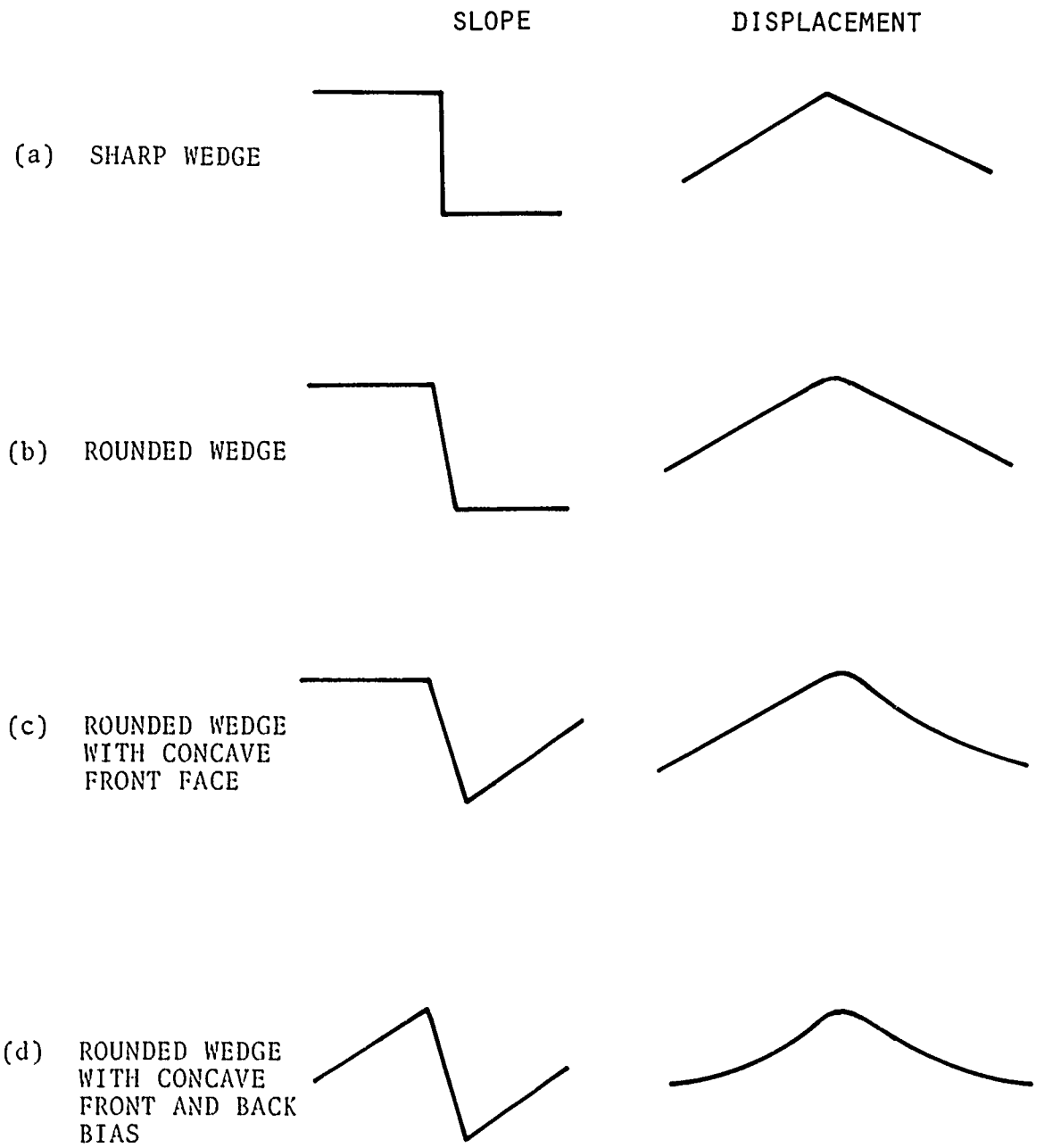

Fig. 20 The model of the "background wave form" can be arrived at from the sharp wedge through a series of deformations.

(a)

(b)

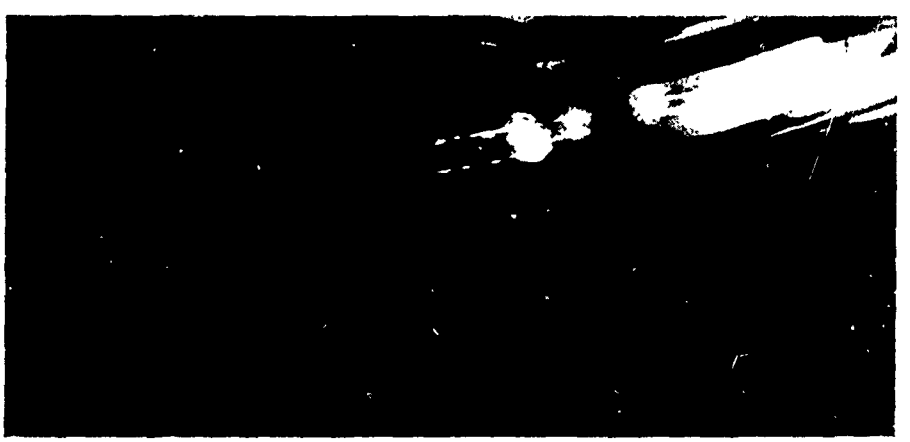

Fig. 21 (a) Point-like specular facets at 55° incidence angle. This is typical for a highly turbulent wake.

(b) Ring-like specular facets at 55° incidence angle. This is typical of very steep capillary waves. The less steep oscillations of the capillaries can be seen in front. z is the cross-tank direction and x is the direction the waves are traveling. The lengths of $\vec{x}$ and $\vec{z}$ vectors represent 2 cm.

APPENDIX 1

THE CONNECTION BETWEEN GTD AND SMALL PERTURBATION THEORY IN THE DESCRIPTION OF WEDGE DIFFRACTION

We will show here that for a small amplitude perfectly conducting wedge, GTD and small perturbation theory produces identical predictions of the backscattering amplitude. As the wedge increases in amplitude, the results start to diverge. As GTD remains valid, this shows that small perturbation theory is breaking down, i.e., the backscattering amplitude is no longer proportional to the resonant Fourier amplitude on the surface.

Consider the wedge shown in Figure A1. The notations and conventions are the same as Barrick et al.[23] (for small perturbation theory) and Beckman[24] (for GTD). In Figure A1, the wedge angle is defined as $(2 - n)\pi$. The incident ray makes an angle x with one face of the wedge and the reflected ray makes an angle ϕ with the same face. In Keller's paper[21], the relevant angles are θ and α which are related to x and θ by:

$$\theta + \frac{\pi}{2} = \phi$$

$$\alpha + \frac{\pi}{2} = x$$

We define the smallness parameter ε by

$$\varepsilon = n - 1.$$

The incidence angle θ_i is then given by

$$\theta_i = (1 + \varepsilon)\frac{\pi}{2} - x.$$

By GTD[24], the wedge diffracts the incident plane wave into a cylindrical wave so that the E-field at an observation point $\vec{r}$ is given by

$$E_r^{\pm} = E_i^{\pm} D^{\pm} f \qquad \text{(A1-1)}$$

where E_r = complex amplitude of reflected E-field at $\vec{r}$

E_i = complex amplitude of incident E-field at the wedge surface

D = diffraction coefficients

f = propagation factors

+ stands for vertical polarization and - stands for horizontal polarization. Thus there is no cross-polarization term in the theory.

The diffraction coefficients are shown[21] to be given by:

$$D^{\pm} = \left[\frac{1}{\cos\left(\frac{\pi}{n}\right) - \cos\left(\frac{\phi - x}{n}\right)} \pm \frac{1}{\cos\left(\frac{\pi}{n}\right) - \cos\left(\frac{\phi + x}{n}\right)} \right] \frac{\sin\left(\frac{\pi}{n}\right)}{n} . \qquad \text{(A1-2)}$$

And the propagation factor f is given by

$$f = \frac{1}{\sqrt{2\pi kr}} e^{i(kr+\pi/4)}$$

where $k = \frac{2\pi}{\lambda}$ = electromagnetic wavenumber

$r = |\vec{r}|$

λ = electromagnetic wave wavelength

The accuracy of formula (A1-2) for describing wedge diffraction is shown in Figure A2. For backscattering, $x = \theta$ so that Equation (A1-1) becomes

$$E_r^{\pm} = E_i^{\pm} \left[\frac{1}{\cos\left(\frac{\pi}{n}\right) - 1} \pm \frac{1}{\cos\left(\frac{\pi}{n}\right) - \cos\left(\frac{2x}{n}\right)} \right] \frac{\sin\left(\frac{\pi}{n}\right)}{n} \frac{1}{\sqrt{2\pi kr}} e^{i(kr+\pi/4)} . \qquad \text{(A1-3)}$$

Now consider the wedge in Figure A1 from the point of view of small perturbation theory. There are usually four restrictions for small perturbation theory[23]:

(i) the roughness height is small compared with wavelength

(ii) surface slopes are relatively small

(iii) the roughness is isotropic

(iv) $L \gg \ell$, the illuminated length is much greater than the surface roughness correlation length.

If h is sufficiently small and L sufficiently large for the wedge in Figure A1, criteria (i) and (ii) are satisfied. (iii) is not essential even for a three-dimensional roughness. Our case here is two-dimensional so that (iii) is not applicable. (iv) is of critical importance for a random surface because the surface Fourier coefficients become uncorrelated in the limit that $L \gg \ell$. Our case here is a deterministic surface so that (iv) is not applicable. The wedge in Figure A1 would therefore be describable by small perturbation theory.

According to Barrick et al.[23], the E-field at an observation point $\vec{r}$ due to a particular scattered mode (m,n) is given by

$$E_r^{\pm}(m,n) = 2kE_i^{\pm}\alpha_{\pm} \cos\theta_i P(m - \nu,n)e^{ia(mx+ny)+ib(m,n)z}$$

where $a = \frac{2\pi}{L}$

$ma = k_x$ = x-component of reflected wavenumber

$na = k_y$ = y-component of reflected wavenumber

ν_a = x - component of incident wavenumber = $k \sin\theta_i$

$\alpha_+ \equiv \alpha_{vv} = \frac{1 + \sin^2\theta_i}{\cos^2\theta_i}$ for backscattering

$\alpha_- = \alpha_{hh} = 1$ for backscattering

$P(m - \nu,n)$ = the $(m - \nu,n)$th Fourier component of the surface.

For our two-dimensional problem here, n = 0. The phase factor can also be written as

$$e^{i\vec{k}_m \cdot \vec{r}}$$

where $\vec{k}_m$ is the reflected wavenumber vector that corresponds to mode m. The total E-field is then the summation over all m:

$$E_r^{\pm}(\vec{r}) = E_i^{\pm} 2k\alpha_{\pm} \cos\theta_i \sum_m P(m - \nu) e^{i\vec{k}_m \cdot \vec{r}}. \qquad \text{(A1-4)}$$

We have to show that for $\varepsilon << 1$, Equation (A1-3) becomes identical to Equation (A1-4).

It is easy to show that the Fourier decomposition of the wedge in Figure A1 is given by

$$y(x) = \frac{h}{2} + \sum_{m = \pm \text{ odd m's}} \frac{2h}{\pi^2 m^2} e^{iamx}.$$

Thus

$$P(m - \nu) = \frac{2h}{\pi^2 (m - \nu)^2} \text{ for } (m - \nu) \text{ odd}.$$

For large L (and thus small a), the summation in Equation (A1-4) can be written as an integral

$$\sum_m P(m - \nu) e^{i\vec{k}_m \cdot \vec{r}} = \int_{-\infty}^{\infty} \frac{1}{2} \frac{2h}{\pi^2 (m - \nu)^2} e^{i\vec{k}_m \cdot \vec{r}} dm.$$

The extra factor of 1/2 is to account for the fact that only odd m modes are counted. It can be seen that the phase factor in the integrand is a rapidly varying function of $\vec{k}_m$. Only wave vectors pointing in the vicinity of $\vec{r}$ will

constructively interfere, i.e., only the modes with $m \sim -\nu$ will contribute to the integral for backscattering. We can therefore write the integral as

$$\left(\frac{1}{2}\right) \frac{2h}{\pi^2(2\nu)^2} \int_{-\infty}^{\infty} e^{i\vec{k}_m \cdot \vec{r}}\, dm.$$

Let the angle between $\vec{k}_m$ and $\vec{r}$ be x, i.e., $x = \theta_r - \theta_m$ if θ_r = angle of $\vec{r}$ and θ_m = angle of $\vec{k}_m$

$$\int_{-\infty}^{\infty} e^{i\vec{k}_m \cdot \vec{r}}\, dm = \int_{-\infty}^{\infty} e^{ikr\cos x} \frac{dm}{dx}\, dx.$$

Since $m = \dfrac{k \sin \theta_m}{a}$

$$\frac{dm}{dx} = \frac{dm}{d\theta_m} \frac{d\theta_m}{dx} = -\frac{k \cos \theta_m}{a} = \frac{-k \cos \theta_i}{a} \text{ for backscattering}$$

$$\int_{-\infty}^{\infty} e^{i\vec{k}_m \cdot \vec{r}}\, dm = -\frac{k \cos \theta_i}{a} \int_{-\infty}^{+\infty} e^{ikr\cos x} dx. \qquad \text{(A1-5)}$$

Expanding cos x as $\left(1 - \frac{x^2}{2}\right)$ and using the argument of the method of stationary phase, (A1-5) becomes

$$-\frac{k \cos \theta_i}{a} \int_{-\infty}^{\infty} e^{ikr(1-x^2/2)} dx$$

$$= -\frac{k \cos \theta_i}{a} e^{ikr} \sqrt{\frac{2\pi}{kr}}\, e^{i(kr+\pi/4)}$$

Equation (A1-4) therefore becomes

$$E_r^{\pm}(\vec{r}) = E_i^{\pm} 2k\alpha_{\pm} \cos\theta_i \frac{h}{\pi^2 4\nu^2} \left(-\frac{k\cos\theta_i}{a}\right) \sqrt{\frac{2\pi}{kr}}\, e^{i(kr+\pi/4)}.$$

Substituting in the expression for $\alpha_{\pm}$, we have

$$E_r^{+}(\vec{r}) = E_i^{+}\left(-\frac{\varepsilon\pi}{2}\right)\left(\frac{1+\sin^2\theta_i}{\sin^2\theta_i}\right)\frac{1}{\sqrt{2\pi kr}}\, e^{i(kr+\pi/4)} \qquad \text{(A1-6)}$$

$$E_r^{-}(\vec{r}) = E_i^{-}\left(-\frac{\varepsilon\pi}{2}\right)\left(\frac{\cos^2\theta_i}{\sin^2\theta_i}\right)\frac{1}{\sqrt{2\pi kr}}\, e^{i(kr+\pi/4)}. \qquad \text{(A1-7)}$$

We now examine the GTD formula, Equation (A1-3), for small ε.

$$\cos\left(\frac{\pi}{n}\right) \sim -1 + O(\varepsilon^2)$$

$$\cos\left(\frac{2x}{n}\right) = -\cos\left(\frac{2\theta}{1+\varepsilon}\right) = -\cos 2\theta' \text{ if } \theta' \equiv \frac{\theta}{1+\varepsilon}$$

$$\frac{\sin\left(\frac{\pi}{n}\right)}{n} \sim \varepsilon\pi.$$

Thus

$$E_r^{+}(r) = E_i^{+}\left(-\frac{\varepsilon\pi}{2}\right)\left(\frac{1+\sin^2\theta'}{\sin^2\theta'}\right)\frac{1}{\sqrt{2\pi kr}}\, e^{i(kr+\pi/4)} + O(\varepsilon^2) \qquad \text{(A1-8)}$$

$$E_r^{-}(r) = E_i^{-}\left(-\frac{\varepsilon\pi}{2}\right)\left(\frac{\cos^2\theta'}{\sin^2\theta'}\right)\frac{1}{\sqrt{2\pi kr}}\, e^{i(kr+\pi/4)} + O(\varepsilon^2). \qquad \text{(A1-9)}$$

For small ε, $\theta' \sim \theta$, the GTD results in Equation (A1-8) and (A1-9) thus agree with the small perturbation results in Equations (A1-6) and (A1-7). We wish

to point out one fine point in our derivation here. In Barrick's[23] analysis, the number of modes that contribute to the E-field at $\vec{r}$ is limited by the angle the surface subtends at $\vec{r}$. For our case, the number of modes is limited to those that remain constructively in phase at r. In usual radar formulations, the observation point is assumed to be in the far field, i.e., $r >> \frac{2L^2}{\lambda}$. It is easy to show that this requirement would imply (actually equivalent to) that Barrick's number of modes is a small subset of ours. However, to make a meaningful comparison between GTD and small perturbation theory, we must remember that the wedge in GTD is supposed to be of infinite extent. The observation point is therefore never in the far field. In fact, $r << \frac{2L^2}{\lambda}$. This means that the number of modes that are in phase at the observation point is a small subset of the number of modes that can be "seen" at the observation point and thus justifies our infinite range of integration rather than Barrick's finite range. The rather incidental phase factor $e^{i\pi/4}$ in GTD is seen to be the familiar one that always appears with the method of stationary phase.

From Equations (A1-8) and (A1-9), we can see that if we wish to use small perturbation theory to describe wedge diffraction, we will have a larger range of applicability if we replace θ in Equation (A1-4) by θ' [$= \theta/(1 + \varepsilon)$]. For large wedge amplitude, the effective incidence angle θ' is smaller. For microwave scattering from the ocean surface, it was observed that as the surface roughens, the polarization ratio becomes smaller (i.e., closer to 0 db). The general accepted notion is that the large waves that tilt the Bragg wave patches are becoming steeper and steeper (and thus reducing the effective incidence angle). However, the rapid increase in steepness required to explain the polarization ratio is too large to be expected from long ocean waves. If microwave backscattering actually comes from small wedge-like waves, it is easy to see

how steepness (i.e., ε) can increase rapidly in short gravity waves, thus reducing θ' and the polarization ratio. (The primary reason may still be the increase in specular reflection, however, as we have discussed in the text.)

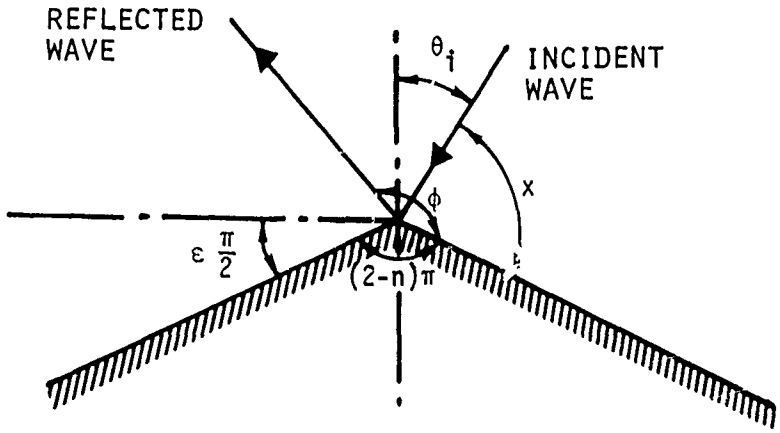

Fig. A1 Conventions for GTD description of wedge diffraction.

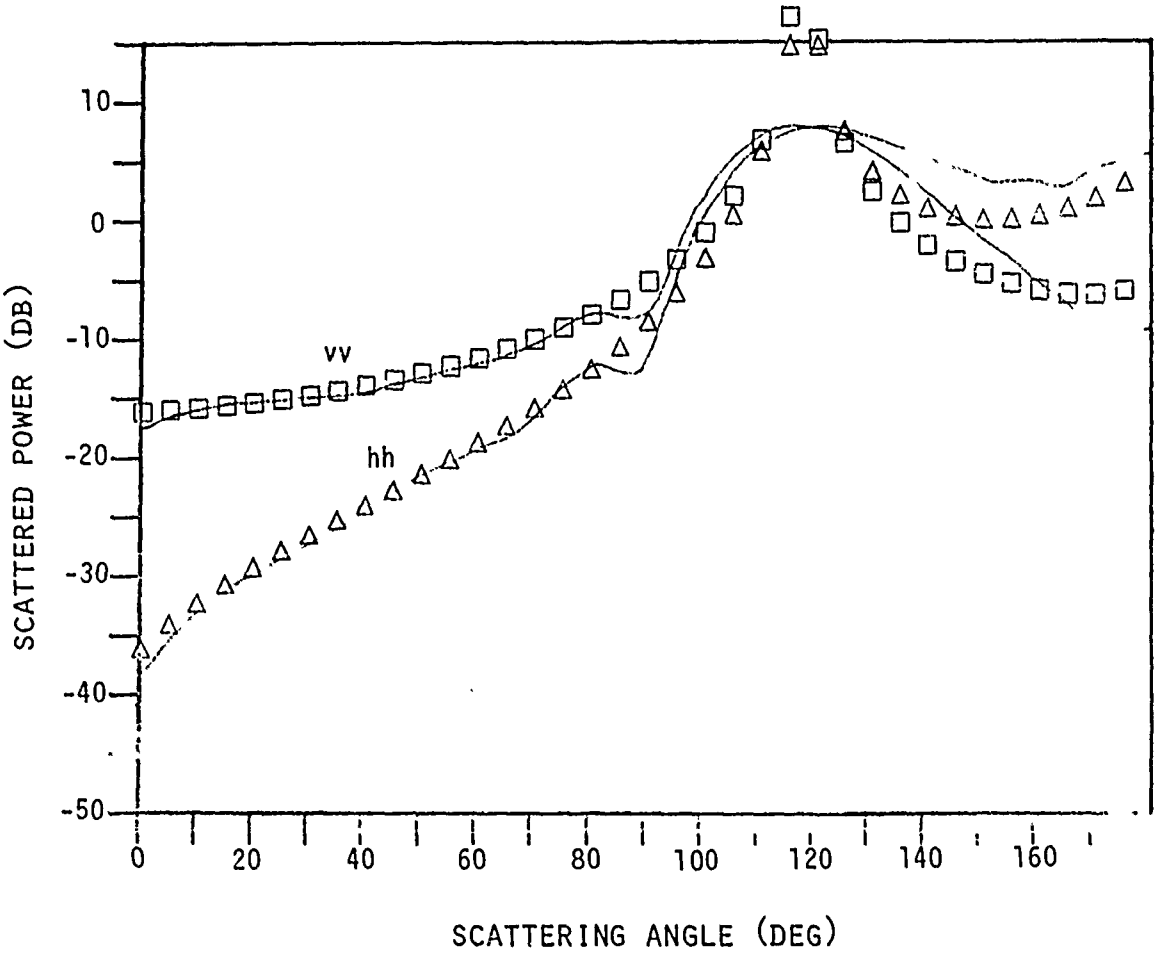

Fig. A2 Scattering for 67.7° incidence angle from a wedge with front slope and back slope both equal to 20° (i.e., $\varepsilon = 2/9$ in Fig. A1). Solid lines — moments method, symbols — GTD (formula A1-2).

APPENDIX 2

SMALL PERTURBATION THEORY FOR A DETERMINISTIC SURFACE

Small perturbation theory is usually formulated for a random surface. However, it is not hard to see from Appendix 1 how it can be easily extended to a deterministic surface. From Equation (A1-4):

$$E_r^{\pm}(\vec{r}) = E_i^{\pm} 2k\alpha_{\pm} \cos\theta_i \sum_m P(m-\nu) e^{i\vec{k}_m \cdot \vec{r}}$$

$$= E_i^{\pm} 2k\alpha_{\pm} \cos\theta_i P(m-\nu) \int e^{i\vec{k}_m \cdot \vec{r}} dm.$$

Again the integral can be evaluated by the method of steepest descent to give $\left(-\frac{k\cos\theta_r}{a}\sqrt{\frac{2\pi}{kr}}\right) e^{i(kr+\pi/4)}$. For comparison with GTD and numerical computations, we normalize with respect to r (i.e., remove r dependence) so that

$$E_r^{+2}(\vec{r}) = \frac{8\pi k^3}{a^2}(1 + \sin\theta_i \sin\theta_r)^2 P^2(m-\nu)$$

$$E_r^{-2}(\vec{r}) = \frac{8\pi k^3}{a^2}\cos^2\theta_i \cos^2\theta_r P^2(m-\nu).$$

Given a surface profile, we can perform a fast Fourier transform whose coefficients are related to $P^2(m-\nu)$ by a numerical constant which can be easily evaluated. We notice that the dependence on k is k^3 rather than the familiar k^4. This is because the computation is in two dimensions. For three dimensions, the integral $\int e^{i\vec{k}\cdot\vec{r}} dmdn$ will produce an extra factor of $\sqrt{\frac{k}{r}}$ so that $E^{\pm 2} \propto \frac{k^4}{r^2}$, i.e., the familiar k^4 dependence and inverse square law.

There is one small precaution that must be taken in trying to apply SPT to a given surface profile. Care must be taken that the profile have the same elevation at both boundaries, i.e., if the profile $y(x)$ has $y(-7.5\lambda_e) = 0$, then $y(+7.5\lambda_e)$ must also be equal to 0. Otherwise, large oscillations due to this mismatch at the periodic boundary will occur in the spectrum if the FFT algorithm used does not have a built-in filter. The precaution is easily overlooked if the input profile is a slope profile. Having zero slope at both boundaries does not guarantee that the elevation will be the same at both boundaries.

REFERENCES

1. Rice, S. O., "Reflection of Electromagnetic Waves from Slightly Rough Surfaces," Comm. Pure Appl. Math. 4, 351-378, 1951.

2. Hasselmann, K., "Weak-Interaction Theory of Ocean Waves" in Basic Developments in Fluid Mechanics, ed. by M. Holt, Academic Press, N.Y., 1968.

3. Keller, W. C. and Wright, J. W., "Microwave Scattering and the Straining of Wind-Generated Waves," Radio Sci. 10, 139-147, 1975.

4. Wright, J. W., "Backscattering from Capillary Waves with Application to Sea Clutter," IEEE Trans. on Ant. and Prop., AP-14, No. 6, 749-754, 1966.

5. Duncan, J. R., Keller, W. C. and Wright, J. W., "Fetch and Wind Speed Dependence of Doppler Spectra," Radio Sci. 9, 809-819, 1974.

6. Lane, F., "Composite-Surface Treatment of the Doppler Spectrum of the Microwave Backscatter from the Ocean Surface at Small Depression Angles," KLD Associates, Inc., TR-34, January 1975.

7. Plant, W. J., and Wright, J. W., "Growth and Equilibrium of Short Gravity Waves in a Wind-Wave Tank," J. Fluid Mech., Vol. 82, Part 4, p. 769, 1977.

8. Plant, W. J., Keller, W. C. and Wright, J. W., "Modulation of Coherent Microwave Backscatter by Shoaling Waves," J. of Geophy. Res., 83-C3, 1347-3152, 1978.

9. Yu, V. Mel-nichuk and Chernikov, A. A., "Spectra of Radar Signals from Sea Surface for Different Polarizations," Atmospheric and Oceanic Physics, Vol. 7, 28-40, 1971.

10. Valenzuela, G. R. and Laing, M. B., "Study of Doppler Spectra of Radar Sea Echo," J. Geophy. Res. 75, 551-563, 1970.

11. Long, M. W., "On a Two-Scatterer Theory of Sea Echo," IEEE Trans. on Ant. and Prop., AP-22, 667-672, 1974.

12. Lewis, J. E. et al., "On the Interaction of Internal Waves and Surface Gravity Waves," J. Fluid Mech., Vol. 63, p. 773, 1974.

13. Lee, P. H. Y., "Doppler Measurements of the Effects of Gravity Waves on Wind-Generated Ripples," J. Fluid Mech., Vol. 81, p. 225, 1977.

14. Love, A. W. ed., "Electromagnetic Horn Antennas," IEEE Press, N. Y., 1976.

15. Morita, T. and Cohn, S. B., "Microwave Lens Matching by Simulated Quarter Wave Transformers," IRE Trans. on Ant. and Prop., 33-39, Jan. 1956.

REFERENCES (Cont.)

16. Chang, J. H. and Wagner, R., "Measurement of Capillary Wave Formation from Steep Gravity Waves," Paper presented at Conference on Atmospheric and Oceanic Waves and Stability of the American Met. Soc., March 29-April 2, Seattle, Washington, 1976.

17. To be published at a later date.

18. Harrington, R. F., Field Computation by Moment Methods, MacMillan, N.Y., 1968.

19. Lentz, R. R., "A Numerical Study of Electromagnetic Scattering from Ocean-like Surfaces," NASA Report CR-2091, 1972.

20. Callan, C. and Dashan, R., "Radar Scattering from the Ocean Surface," Vol. II, JASON 1968 Summer Study.

21. Keller, J. B., "Geometric Theory of Diffraction," J. Opt. Soc. Am., Vol. 52, p. 116-130 (1962).

22. Saxton, J. A. and Lane, J. A., "Electrical Properties of Sea Water," Wireless Engineer, 269-275, Oct. 1952.

23. Barrick, D. E. and Peak, W. H., "Scattering from Surfaces with Different Roughness Scales: Analysis and Interpretation," Battelle Mem. Inst. Report BAT-197A-10-3, 1967.

24. Beckmann, P., "The Depolarization of Electromagnetic Waves," The Golam Press, Boulder, CO, 1968.

DISTRIBUTION:

Office of Naval Research
800 North Quincy Street
Arlington, VA 22217
Attn: Mr. Hans Dolezalek, Code 422CS

1 Copy

Office of Naval Research
Western Regional Office
1030 East Green Street
Pasadena, CA 91106

1 Copy

Administrative Contracting Officer (ResRep,DCASMA)

1 Copy

Director, Naval Research Laboratory
Attn: Code 2627
Washington, D.C. 20375

6 Copies

Defense Technical Information Center
Bldg. 5, Cameron Sta.
Alexandria, VA 22314

12 Copies

Robert C. Beal
APL/JHU
Johns Hopkins Road
Laurel, MD 20707

Dr. Wolfgang Boerner
University of Illinois at Chicago Circle
Chicago, Illinois

Rod. R. Buntzen
Code 1603, NOSC
San Diego, CA 92151

Prof. Dr. Klaus Hasselmann
Max Planck Institut f. Meteorologie
Bundes Strasse 55
D-2000 Hamburg 13
West Germany

Dr. Atul Jain
Mail Stop 183-501
Jet Propulsion Laboratory
4800 Oak Grove Drive
Pasadena, CA 91130

Dr. D. W. S. Lodge
Remote Sensing Applications & Research Station
Procurement Executive, Ministry of Defense, Royal Aircraft Establishment, Space Department
Farnborough, Hampshire
England

Dr. Richard K. Moore
The University of Kansas Center for Research, Inc.
2291 Irving Hill Drive, Campus West
Lawrence, KS 66045

Dr. William Plant
Code 4305
Naval Research Laboratory
Washington, D.C. 20375

Dr. Keith Raney
Canadian Center for Remote Sensing
2464 Sheffield Road
Ottawa, Ontario, K1A 0Y7
Canada

Dr. Omar H. Shemdin
Jet Propulsion Laboratory
4800 Oak Grove Drive
Pasadena, CA 91130

Dr. Robert A. Shuchman
Manager, Radio Remote Sensing Program
Environmental Research Institute of Michigan
P.O. Box 8618
Ann Arbor, Michigan 48107

Dr. Gordon Smith
APL/JHU
Johns Hopkins Road
Laurel, MD 20707

Dr. Dennis B. Trizna
Code 5320
Naval Research Laboratory
Washington, D.C. 20375

Dr. Gaspar R. Valenzuela
Code 4305
Naval Research Laboratory
Washington, D.C. 20375